Analysis of interaction between cellulosic biomass and saccharification enzymes

Makiko Imai

2020

Contents

Chapter 1 General Introduction 1

1.1 Background 1

1.1.1 Biomass and Bioenergy 1

1.1.2 Bioethanol 2

1.1.3 Cellulose 4

1.1.4 Enzymes 5

1.1.5 Problems of saccharification in bioethanol production 7

1.2 Purpose of this study 7

1.3 References 8

Chapter 2 Analysis of sugarcane bagasse cellulose residue of saccharification 12

2.1 Introduction 12

2.2 Materials and Methods 13

2.2.1 Preparation of bagasse cellulose 13

2.2.2 Enzymatic hydrolysis 13

2.2.3 Degree of polymerization 14

2.2.4 TEM 14

2.2.5 SAXS measurement 14

2.2.6 Acquisition of IR spectra for deuterated bagasse cellulose 15

2.3 Results and Discussion 16

2.3.1 Enzymatic hydrolysis 16

2.3.2 Weight-averaged DP 17

2.3.3 TEM 17

2.3.4 SAXS analysis 20

2.3.5 IR spectra of deuterated bagasse cellulose 21

2.4 Conclusions 25

2.5 List of abbreviations 26

2.6 References 26

Chapter 3 Direct observation of cellulase penetration in oven-dried pulp by confocal laser scanning microscopy 30

3.1 Introduction 30

3.2 Materials and methods 31

3.2.1 Pulps 31

3.2.2 Measurement of pulp width 31

3.2.3 Enzymatic Hydrolysis 32

3.2.4 Labeling of enzyme with fluorescence dye 32

3.2.5 Observation of enzyme penetration to pulps 33

3.2.6 Immunofluorescence microscopy for hemicellulose detection 34

3.3 Results and discussion 34

3.3.1 Optical microscopic observation of pulp 34

3.3.2 Measurement of the width of pulp fibers 35

3.3.3 Enzymatic Hydrolysis 36

3.3.4 Observation of the penetration of cellulase 38

3.3.5 Xylan and Mannan distribution on ND and ODr pulp 42

3.4 Conclusion 45

3.5 List of abbreviations……45

3.6 References……45

Chapter 4 Time-lapse enzyme visualization during sugarcane hydrolysis 49

4.1 Introduction……49

4.2 Materials and Methods……..50

4.2.1 Enzyme preparation 50

4.2.2 Enzyme labeling with a fluorescent dye.....51

4.2.3 Assessment of labeled xylanases 51

4.2.4 Fluorescence microscopy of a selectively-labeled enzyme in a cellulase cocktail……52

4.2.5 Relationship between the number of labeled enzymes and fluorescence image intensity……..53

4.2.6 Time-lapse fluorescence profiles from two-dimensional images……53

4.3 Results and discussion……54

4.3.1 Xylanase activity: effect of labeling 54

4.3.2 Relationship between the number of labeled enzymes and fluorescence image intensity ……..56

4.3.3 Changes to morphology and enzyme adsorption during hydrolysis.....57

4.3.4 Time-lapse analysis of individual enzymes 58

4.3.5 Time-lapse analyses of enzyme activity in specific anatomical area 61

4.4 Conclusions……..64

4.5 List of abbreviations……..64

4.6 References……65

Chapter 5 Summary 69

Acknowledgement 71

Contents

Chapter 1 General Introduction

1.1 Background

1.1.1 Biomass and Bioenergy

Biomass originally meant the mass of living organisms. In recent years, the word "biomass" is often used to refer to living organisms material used for energy production. Biomass has received attention as an alternative energy resource for fossil fuels. Numerous studies have been conducted and some biomass energy sources are commercially available.

Biomass is classified as crops (e.g. corn and sugarcane) and other resources. Other resources are generally classified as agricultural wastes (e.g. straw, bagasse, and corn stover), forest wastes (e.g. saw dust, pulp waste, and thinned wood), municipal

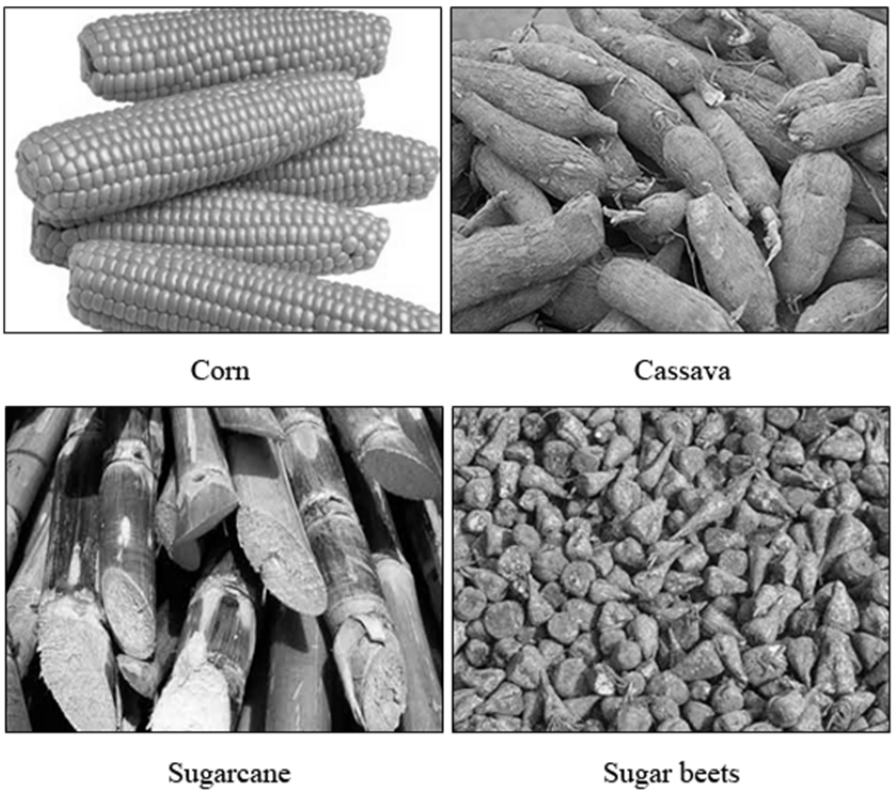

Figure 1.1 Examples of first generation feedstocks (cited from the University of Hawaii webpage)

waste, and industrial waste. Edible feedstocks are first generation (Fig. 1.1), and second generation feedstocks do not compete with food (Fig. 1.2). Third generation feedstocks are microalgae. Biomass has several uses (e.g. combustion, gasification, and chemical) and forms (e.g. biodiesel, methane, ethanol) (Naik et al. 2010). The development of new alternative sources of energy is a topic of extensive research around the world. The exhaustion of petroleum supplies and global warming by greenhouse gases require that energy sources evolve from fossil resources to bioresources. Recently a wealth of interdependent research has focused on the use of inedible biomass such as lignocellulose.

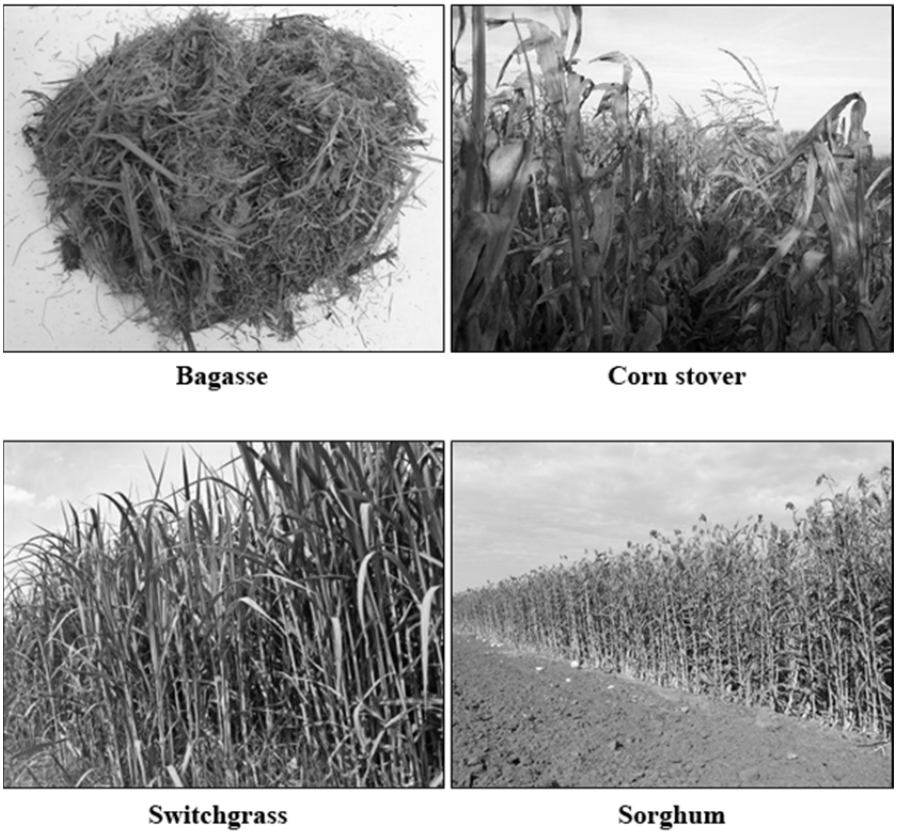

Figure 1.2 Examples of second generation feedstocks (cited from the University of Hawaii webpage)

1.1.2 Bioethanol

In this study, enzymatic saccharification was the focus during bioethanol production. Bioethanol is a primary bioenergy source and is produced from biomass, such as corn, sugarcane, nepia grass, wood chips, and wood pulp.

The main usage of bioethanol is as a fuel for vehicles. Brazil is one of the largest producer of bioethanol in the world, with the main material being sugarcane juice (Amorim et al. 2011). The USA started producing bioethanol from corn in the 1970s, and has surpassed Brazil in the level of production (Saini et al. 2016). Both corn and sugarcane are food or livestock feed and the their usage as bioethanol conflicts with the demand for food. Biofuels produced from food are called first-generation biofuels .

Biofuels from non-food materials have been developed in some countries, including Japan, and they are considered second-generation biofuels (Fig. 1.3). The second generation consists of such materials as thinned wood, wood chips, corn stover, bagasse, rice straw, waste paper, and weeds (Naik et al. 2010).

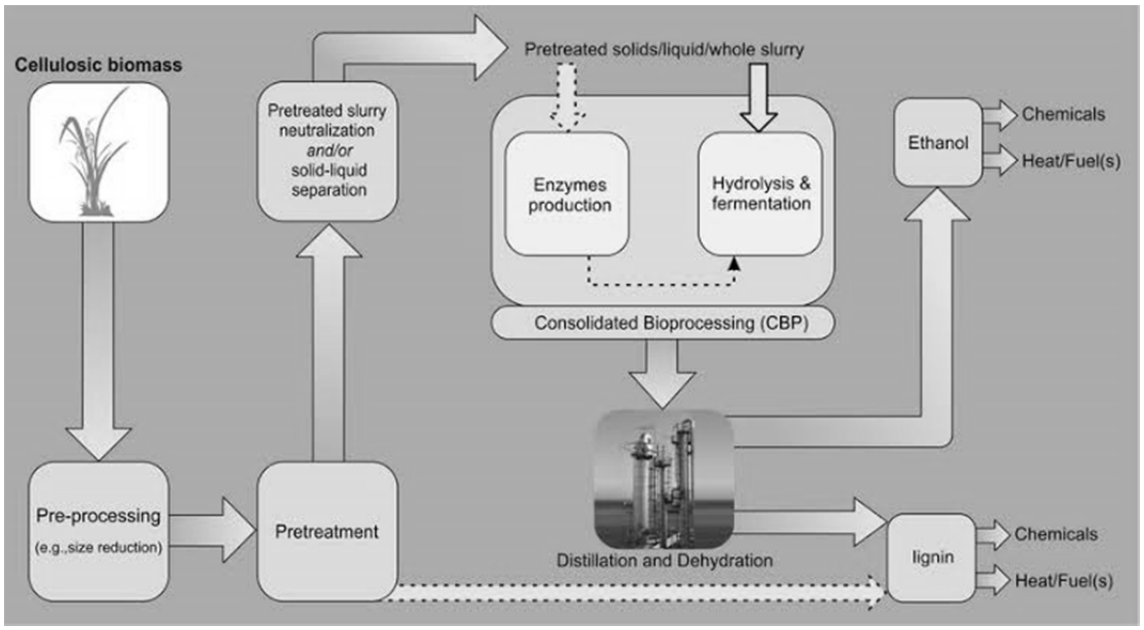

Figure 1.3 Schematic of the second-generation ethanol production process (from Kumar et al.)

In Japan, the adaptation of bioethanol was determined in Kyoto Protocol Target Achievement Plan in 2005, and bioethanol from cellulosic biomass of the second generation has been studied (Matsumoto et al. 2009). DINS Sakai (recycler) produces bioethanol from waste wood chips. However, there are only a few full-scale plants of bioethanol in Japan.

To produce bioethanol from cellulosic biomass, cellulose and hemicellulose must be hydrolyzed to monosaccharides. There are two methods of cellulose hydrolysis, acid hydrolysis and enzymatic hydrolysis. Research and development of enzymatic hydrolysis of cellulose is in the mainstream because acid hydrolysis has some associated problems, e.g., corrosion of the plant and energy during acid recovery, and a high temperature requirement for diluting the acid (Galbe and Zacchi 2002).

1.1.3 Cellulose

Cellulose, which is the most abundant biomass on earth, is a main component of woody biomass and herbaceous biomass (Marchessault and Sundararajan 1983). Cellulose is a linear chain polysaccharide of several hundred to many thousands of β (1→4) linked D-glucose units. Cellulose is insoluble in water and in most organic

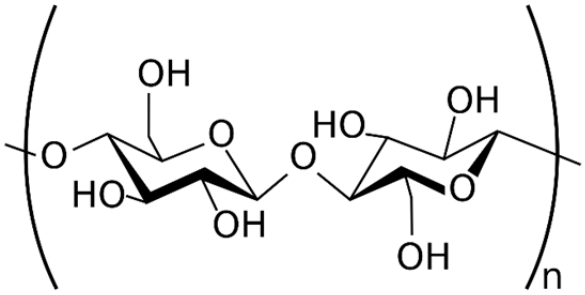

Figure 1.4 Cellulose molecule

solvents (Fig. 1.4).

Native cellulose (cellulose I) has a structural diversity depending on species, such as allomorphism (I_α/I_β or a triclinic/monoclinic two-phase model) (Atalla and Vanderhart 1984), later identified as triclinic/monoclinic two individual crystalline moieties (Sugiyama et al. 1991), dimension (Preston and Cronshaw 1958), and uniplanar orientation behavior of the specific crystallographic plane to the cell wall surface (Koyama et al. 1997b). The “parallel-up” packing in cellulose I_α and I_β unit

cells was experimentally demonstrated by a combination of directly staining the reducing ends of the cellulose chains and microdiffraction tilting electron crystallographic analysis (Fig. 1.5) (Koyama et al. 1997a), and was later confirmed by X-ray and neutron diffraction crystallography (Nishiyama et al. 2002, 2003). These native cellulose allomorphs are packed in crystalline phases by unique intra- and inter-hydrogen networks to ether, with a hydrophobic interaction between cellulose molecules (Nishiyama et al. 2002, 2003). Many crystal models of cellulose have been published so far, but the ones from the Sarko's group (Sarko and Muggli 1974;

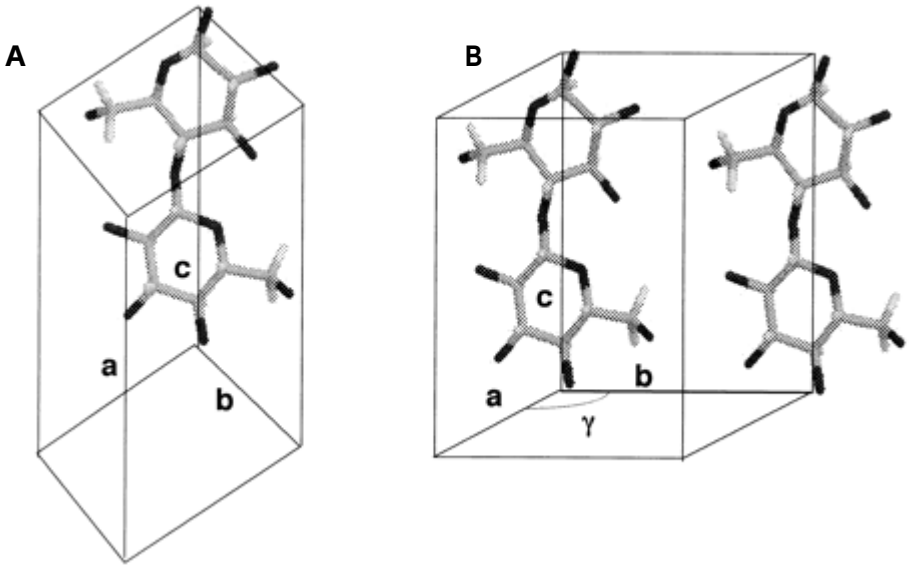

Figure 1.5 Schematic representation of the mode of chain packing in the unit cell of cellulose. (*A*) Triclinic unit cell. (*B*) Monoclinic unit cell. Monoclinic angle γ is obtuse (Koyama et al. 1997a).

Woodcock and Sarko 1980) are the closest to the current models.

1.1.4 Enzymes

Cellulase and hemicellulase are used in the enzymatic hydrolysis of lignocellulosic biomass. The enzymes are biosynthesized by fungi, bacteria, plants, and animals .

These enzymes are cocktails of some enzyme components (Sheir-Neiss and Montenecourt 1984). The main components are cellobiohydrolase (CBH),

endoglucanase (EG), and β-glucosidase (GBL). CBH I is the most abundant in many cellulase cocktail and it processively hydrolyzes celluloses from their reducing ends. Another processive enzyme, CBH II works from the nonreducing ends of celluloses. EGs attack amorphous cellulose at random and β-glucosidase converts a cellooligosaccharides into glucoses (Fig. 1.6). These enzyme components act synergistically to degrade celluloses to glucoses (Henrissat et al. 1985; Beldman et al. 1988; Wood et al. 1989).

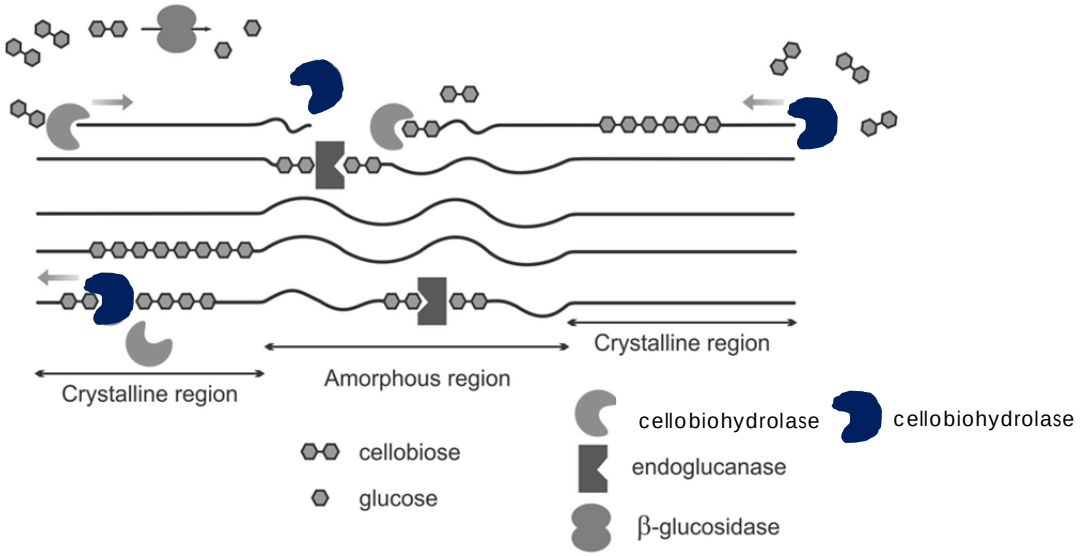

Figure 1.6 Simplified schematic representation of the enzymatic action of cellulase, involving cellobiohydrolase, endoglucanase and β-glucosidase, on cellulose (modified of Akhtar et al. 2016)

Trichoderma, a kind of filamentous fungi with a high productivity of cellulase, has been studied and its cellulase has been commercially produced in some countries (Samuels 1996). This study was done within the frame work of "Construction of Innovative Saccharifying Enzyme producing Microorganism and Development of Manufacturing of the Enzyme for the Biofuel Commercialization" and "Demonstration and Development Project of Production System for Cellulosic Bioethanol/Development of Technologies for Integrated Production from Woody Biomass of Cellulosic Ethanol that meets the Japanese standard for sustainability and

Feasibility Study" of the New Energy and Industrial Technology Development Organization (NEDO). In NEDO projects, mutant and recombinant strains of *Trichoderma reesei*, which have higher activity to lignocellulose than the wild type, have been developed (Nakazawa et al. 2012; Kawai et al. 2012; Matsuzawa et al. 2016). However, these enzymes are expensive and cost is one of the most difficult problems to overcome in producing bioethanol (Banerjee et al. 2010; Acharya and Chaudhary 2012). As solutions, recycling of enzymes (Rodrigues et al. 2012; Haven et al. 2015) and pretreatment of biomass for a lower enzyme loading hydrolysis have been investigated (Banerjee et al. 2010).

1.1.5 Problems of saccharification in bioethanol production

There are some problems in the hydrolysis of cellulosic biomass. Woody and herbaceous biomass contain lignin, which inhibits the hydrolysis of cellulose and hemicellulose because of a restriction of accessibility and non-productive adsorption (Berlin et al. 2006; Rahikainen et al. 2011). Thus, the efficient pretreatment of biomass is the first important step in the hydrolysis of lignocellulosic biomass. Another serious problem is the cost of enzymes, as mentioned before. The yield of saccharification, however, reaches the limit when the enzyme loading is decreased to a few milligrams of enzyme per gram of substrate. Dozens of milligrams of enzyme per gram of substrate are necessary for complete hydrolysis (Horikawa et al. 2013).

1.2 Purpose of this study

When the saccharification yield reaches the limit, the interactions between biomass (substrate) and enzymes are still unclear. It is indispensable to improve enzymes and biomass to saccharify cellulosic biomass efficiently using a small number of enzymes.

In this study, focusing on cellulosic biomass, the author tried to analyze the structure of substrate residue on the limit of saccharification, and to reveal the interaction between the biomass and enzymes during saccharification using a small number of enzymes. The ultimate goal is to propose the ideal biomass for producing bioethanol.

1.3 References

Acharya S, Chaudhary A (2012) Bioprospecting thermophiles for cellulase production: a review. Braz J Microbiol 43:844–856. https://doi.org/10.1590/S1517-83822012000300001

Amorim HV, Lopes ML, de Castro Oliveira JV, et al (2011) Scientific challenges of bioethanol production in Brazil. Appl Microbiol Biotechnol 91:1267–1275. https://doi.org/10.1007/s00253-011-3437-6

Atalla RH, Vanderhart DL (1984) Native Cellulose: A composite of two distinct crystalline forms. Science 223:283–285. https://doi.org/10.1126/science.223.4633.283

Banerjee S, Mudliar S, Sen R, et al (2010) Commercializing lignocellulosic bioethanol: technology bottlenecks and possible remedies. Biofuels Bioprod Biorefining 4:77–93. https://doi.org/10.1002/bbb.188

Beldman G, Voragen AG, Rombouts FM, Pilnik W (1988) Synergism in cellulose hydrolysis by endoglucanases and exoglucanases purified from Trichoderma viride. Biotechnol Bioeng 31:173–178. https://doi.org/10.1002/bit.260310211

Berlin A, Balakshin M, Gilkes N, et al (2006) Inhibition of cellulase, xylanase and β-glucosidase activities by softwood lignin preparations. J Biotechnol 125:198–209. https://doi.org/10.1016/j.jbiotec.2006.02.021

Galbe M, Zacchi G (2002) A review of the production of ethanol from softwood. Appl Microbiol Biotechnol 59:618–628. https://doi.org/10.1007/s00253-002-1058-9

Gunjikar TP, Sawant SB, Joshi JB (2001) Shear deactivation of cellulase, exoglucanase, endoglucanase, and beta-glucosidase in a mechanically agitated reactor. Biotechnol Prog 17:1166–1168. https://doi.org/10.1021/bp010114u

Haven MØ, Lindedam J, Jeppesen MD, et al (2015) Continuous recycling of enzymes during production of lignocellulosic bioethanol in demonstration scale. Appl Energy 159:188–195. https://doi.org/10.1016/j.apenergy.2015.08.062

Henrissat B, Driguez H, Viet C, Schülein M (1985) Synergism of cellulases from *Trichoderma reesei* in the degradation of cellulose. Nat Biotechnol 3:722–726. https://doi.org/10.1038/nbt0885-722

Horikawa Y, Konakahara N, Imai T, et al (2013) The structural changes in crystalline cellulose and effects on enzymatic digestibility. Polym Degrad Stab 98:2351–2356. https://doi.org/10.1016/j.polymdegradstab.2013.08.004

Kawai T, Nakazawa H, Ida N, et al (2012) Analysis of the saccharification capability of high-functional cellulase JN11 for various pretreated biomasses through a comparison with commercially available counterparts. J Ind Microbiol Biotechnol 39:1741–1749. https://doi.org/10.1007/s10295-012-1195-9

Koyama M, Helbert W, Imai T, et al (1997a) Parallel-up structure evidences the molecular directionality during biosynthesis of bacterial cellulose. Proc Natl Acad Sci U S A 94:9091–9095

Koyama M, Sugiyama J, Itoh T (1997b) Systematic survey on crystalline features of algal celluloses | SpringerLink. Cellulose 4:147–160

Kumar R, Tabatabaei M, Karimi K, Sárvári Horváth I (2016) Recent updates on lignocellulosic biomass derived ethanol - A review. Biofuel Res J 3:347–356. https://doi.org/10.18331/BRJ2016.3.1.4

Marchessault RH, Sundararajan PR (1983) 2 - Cellulose. In: Aspinall GO (ed) The Polysaccharides. Academic Press, pp 11–95

Matsumoto N, Sano D, Elder M (2009) Biofuel initiatives in Japan: Strategies, policies, and future potential. Appl Energy 86:S69–S76. https://doi.org/10.1016/j.apenergy.2009.04.040

Matsuzawa T, Kaneko S, Yaoi K (2016) Improvement of thermostability and activity of *Trichoderma reesei* endo-xylanase Xyn III on insoluble substrates. Appl Microbiol Biotechnol 100:8043–8051. https://doi.org/10.1007/s00253-016-7563-z

Naik SN, Goud VV, Rout PK, Dalai AK (2010) Production of first and second generation biofuels: A comprehensive review. Renew Sustain Energy Rev 14:578–597. https://doi.org/10.1016/j.rser.2009.10.003

Nakazawa H, Kawai T, Ida N, et al (2012) Construction of a recombinant *Trichoderma reesei* strain expressing Aspergillus aculeatus β-glucosidase 1 for efficient biomass conversion. Biotechnol Bioeng 109:92–99. https://doi.org/10.1002/bit.23296

Nishiyama Y, Langan P, Chanzy H (2002) Crystal structure and hydrogen-bonding system in cellulose Iβ from synchrotron X-ray and neutron fiber diffraction. J Am Chem Soc 124:9074–9082. https://doi.org/10.1021/ja0257319

Nishiyama Y, Sugiyama J, Chanzy H, Langan P (2003) Crystal structure and hydrogen bonding system in cellulose Iα from synchrotron X-ray and neutron fiber diffraction. J Am Chem Soc 125:14300–14306. https://doi.org/10.1021/ja037055w

Rahikainen J, Mikander S, Marjamaa K, et al (2011) Inhibition of enzymatic hydrolysis by residual lignins from softwood—study of enzyme binding and inactivation on lignin-rich surface. Biotechnol Bioeng 108:2823–2834. https://doi.org/10.1002/bit.23242

Rodrigues AC, Leitão AF, Moreira S, et al (2012) Recycling of cellulases in lignocellulosic hydrolysates using alkaline elution. Bioresour Technol 110:526–533. https://doi.org/10.1016/j.biortech.2012.01.140

Saini JK, Patel AK, Adsul M, Singhania RR (2016) Cellulase adsorption on lignin: A roadblock for economic hydrolysis of biomass. Renew Energy 98:29–42. https://doi.org/10.1016/j.renene.2016.03.089

Samuels GJ (1996) *Trichoderma*: a review of biology and systematics of the genus. Mycol Res 100:923–935. https://doi.org/10.1016/S0953-7562(96)80043-8

Sheir-Neiss G, Montenecourt BS (1984) Characterization of the secreted cellulases of *Trichoderma reesei* wild type and mutants during controlled fermentations. Appl Microbiol Biotechnol 20:46–53. https://doi.org/10.1007/BF00254645

Wood TM, McCrae SI, Bhat KM (1989) The mechanism of fungal cellulase action. Synergism between enzyme components of *Penicillium pinophilum* cellulase in solubilizing hydrogen bond-ordered cellulose. Biochem J 260:37–43

Chapter 2 Analysis of sugarcane bagasse cellulose residue of saccharification

2.1 Introduction

Sugarcane has been cultivated to produce sugar for a long time. Increasing amounts of sugarcane have been used to produce bioethanol over the past few decades. Producing bioethanol from cellulose economically requires saccharification to be achieved using the minimum dosage of enzymes. However, cellulose I (native cellulose) is not completely saccharified to glucose at a low cellulase concentration (Horikawa et al. 2013). It has been suggested in numerous studies that the low saccharification rate is caused by the non-specific adsorption of enzymes to substrates (making the enzymes inactive) (Grethlein and Converse 1991; Palonen et al. 2004; Lou et al. 2013; Saini et al. 2016), enzyme deactivation through other processes (Gunjikar et al. 2001), inhibition caused by the products (Atreya et al. 2016), and the effects of certain cellulose characteristics. It has been suggested that problems of low saccharification rates may be related to using substrates with high hemicellulose contents, high lignin contents, and certain surface pore sizes (Grethlein and Converse 1991), but the saccharification rate is low at a low cellulase concentration even for pure cellulose I (with hemicellulose and lignin removed). However, cellulose III_I is almost completely hydrolyzed at low enzyme concentrations (Horikawa et al. 2013). Cellulose III_I is produced from cellulose I but has a different crystalline form from cellulose I (Wada et al. 1997). The saccharification limit is therefore caused by a combination of the hemicellulose and lignin contents and the cellulose I structure.

In the study described here, cellulose residues after saccharification were analyzed, because the author assumed that a poor saccharification rate was related to the structures of the residue. Cellulose residues were first analyzed by transmission electron microscopy (TEM) and by making small angle X-ray scattering (SAXS) measurements to assess the morphologies of the residues. Cellulose residues were then deuterated to allow the hydrophilicities of the residues to be determined. Cellulose has been deuterated in numerous previous studies. Infra-red (IR) spectra of the deuterated

cellulose were acquired. The OH stretching bands at 3500–3300 cm^{-1} were completely translated to wavelengths ~1000 cm^{-1} lower without any loss of resolution (Nishiyama et al. 1999), and the deuteration ratio was easily determined (Horikawa and Sugiyama 2008). Only OH groups on the surfaces and in disordered regions are deuterated when cellulose is stored in deuterium oxide (Hofstetter et al. 2006), but OH groups even in crystalline regions are deuterated when cellulose is treated with a sodium deuteroxide solution at a high temperature and a high pressure (Wada et al. 1997). In the study described here, a saccharification residue was stored in deuterium oxide under conditions that caused only OH groups on the surfaces and in disordered regions to become deuterated, to allow the residue surfaces to be analyzed.

2.2 Materials and Methods

2.2.1 Preparation of bagasse cellulose

Sugarcane bagasse powder that had been passed through a 1 mm sieve was treated with acidified sodium chlorite solution at 70 °C using The Jayme–Wise method (Wise et al. 1946). This process was repeated five times until IR absorption bands at 1510 and 1600 cm^{-1} (assigned to aromatic skeletal vibrations of the lignin) had completely disappeared. The sample was then boiled in 5% sodium hydroxide for 2 h to remove hemicellulose. Obtained samples were then processed twice by using a disk mill to be fibrillated.

2.2.2 Enzymatic hydrolysis

The enzyme Accellerase1500 (DuPont, Wilmington, DE, USA) was used in the study. Accellerase1500 is produced using a genetically modified strain of *Trichoderma reesei*. Bagasse cellulose (10 mg on a dry matter basis) was placed in a test tube, then 1 mL of 100 mM acetate buffer (pH 5.0) and 10 μg of Accellerase1500 were added. The mixture was incubated at 50 °C in a water bath with shaking at 150 rpm. The D-glucose concentration in the supernatant was measured 1, 24, 72, 142, 168, and 196 h after incubation started using a D-glucose assay kit (Roche, Basel, Switzerland). The saccharification rate was defined as the ratio between the measured amount of glucose

and the total amount of glucose calculated from the amount of cellulose present, expressed as a percentage.

2.2.3 Degree of polymerization

The weight-averaged molecular weight of cellulose was estimated using the method described by Horikawa et al. (2016) modified as described by Hallac et al. (2009). Cellulose was derivatized using a tricarbanilation process performed using anhydrous pyridine and phenyl isocyanate. The products were dissolved in tetrahydrofuran, and the soluble material was subjected to the procedure described below. Gel permeation chromatography analysis was performed at 40 °C on a Shodex GPC-101 using a high-speed liquid chromatography system (Shoko Co., Ltd., Kanagawa,Japan) equipped with a guard column (Shodex GPC KF-G), two 30 cm mixed columns (Shodex GPC KF-806L), and a differential refractometer (Shodex RI-101). Calibration curves were produced using polystyrene standards. The degree of polymerization (DP) was calculated by dividing the weight-averaged molecular weight by 519 (the molecular weight of the cellulose tricarbanilate repeating unit).

2.2.4 TEM

The cellulose residue after enzymatic hydrolysis had been performed was washed thoroughly with distilled water and suspended in water. The suspension was then applied to a grid covered with carbon. Excess water was removed with a filter paper, then the grid was negatively stained with 2% uranyl acetate. Photographs of the sample were acquired using a 2000EX TEM system (JEOL, Tokyo, Japan) using a voltage of 100 kV.

The lengths and widths of the cellulose microfibril residues after hydrolysis for 1, 24, and 196 h were determined from the TEM images using Image J software.

2.2.5 SAXS measurement

Slurries of nanofibrillated cellulose before and after enzymatic hydrolysis for 142 h were subjected to SAXS measurements using the BL8S3 beamline at the Aichi Synchrotron Radiation Center (Aichi, Japan). The cellulose concentrations in the slurries of the samples that had been hydrolyzed for 0 and 142 h, determined using the anthrone–sulfuric acid reaction described previously (Imai et al. 2014), were ~0.39% w/v and ~0.24% w/v, respectively. To perform a measurement, a slurry sample was loaded into a liquid cell (made in-house) with a 3 mm optical path and 0.02 mm thick

quartz plate windows. The cell was placed in a temperature-controlled sample holder. SAXS measurements were performed using X-rays with an energy of 13.5 keV (wavelength 0.092 nm) and a sample-to-camera distance of 2.1 m. The parameters relating to the geometry of the experiment were calibrated using silver behenate. A scattering pattern was recorded using an R-Axis IV++ imaging plate detector (Rigaku, Tokyo, Japan) using a 600 s exposure time. Azimuthal integration of the scattering pattern was performed using the beamline program to give one-dimensional data for the scattering intensity (I) based on the scattering vector $q = (4\pi \cdot \sin \theta)/\lambda$. The intensity was normalized by the X-ray absorbance estimated from the photon count measured using ionizing chambers in front of and behind the sample. The one-dimensional data were visualized and analyzed using Python 3.7.0 software.

2.2.6 Acquisition of IR spectra for deuterated bagasse cellulose

Saccharification residues after 0, 24, 72, and 196 h of incubation were treated with 0.2% sodium hydroxide to remove the enzymes, then each sample was washed thoroughly with distilled water. Each sample was then washed twice with deuterium oxide (99.9% D atoms; Sigma-Aldrich, St. Louis, MO, USA) and then stored in deuterium oxide at room temperature for 24 h.

The Fourier-transform (FT) IR spectrum of each sample was acquired using a Frontier FT-IR spectrometer (PerkinElmer, Waltham, MA, USA). The wave number range for a spectrum was 500–4000 cm^{-1}, and the resolution was 4 cm^{-1}. For each spectrum, 16 scans were performed in attenuated total reflection (ATR) mode. The ATR prism was covered with a plastic petri dish with a small hole in the center (Fig. 2.1). The cellulose suspension to be analyzed (2.5 μL) was applied to the ATR prism through the hole. Ultra-high purity nitrogen that had been passed through a liquid nitrogen trap was blown over the sample from the hole to dry it. An IR spectrum was acquired 5 min after the absorbance characteristics of deuterium oxide were last detected. The spectrum was smoothed and base-line corrected, then the spectrum was normalized to the heights of the CH and CH_2 absorbance peaks. The OD ratio was calculated using the equation shown below (Horikawa and Sugiyama 2008).

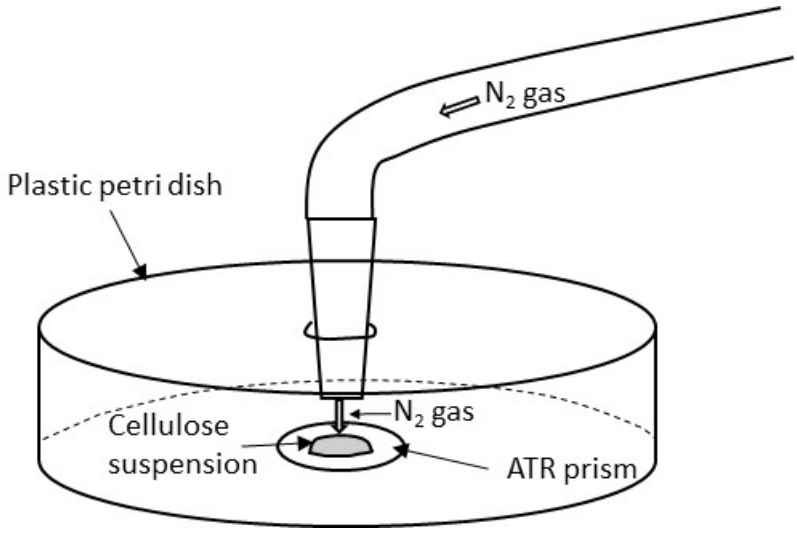

Figure 2.1 Schematic of the apparatus used to acquire an infra-red spectrum in attenuated total reflection mode

OD ratio (%) = $100 \times (A_{OD} / (A_{OH} + A_{OD}))$

A_{OD} = height of the OD absorbance peak (~2500 cm^{-1})

A_{OH} = height of the OH absorbance peak (~3330 cm^{-1})

2.3 Results and Discussion

2.3.1 Enzymatic hydrolysis

It has previously been found that cellulose is not completely enzymatically hydrolyzed at low cellulase concentrations (Horikawa et al. 2013). In this study, the saccharification rate reached a maximum at 142 h (Fig. 2.2), as was found previously (Horikawa et al. 2013). The saccharification rate was lower at 196 h than at 168 h, but the difference was not significant.

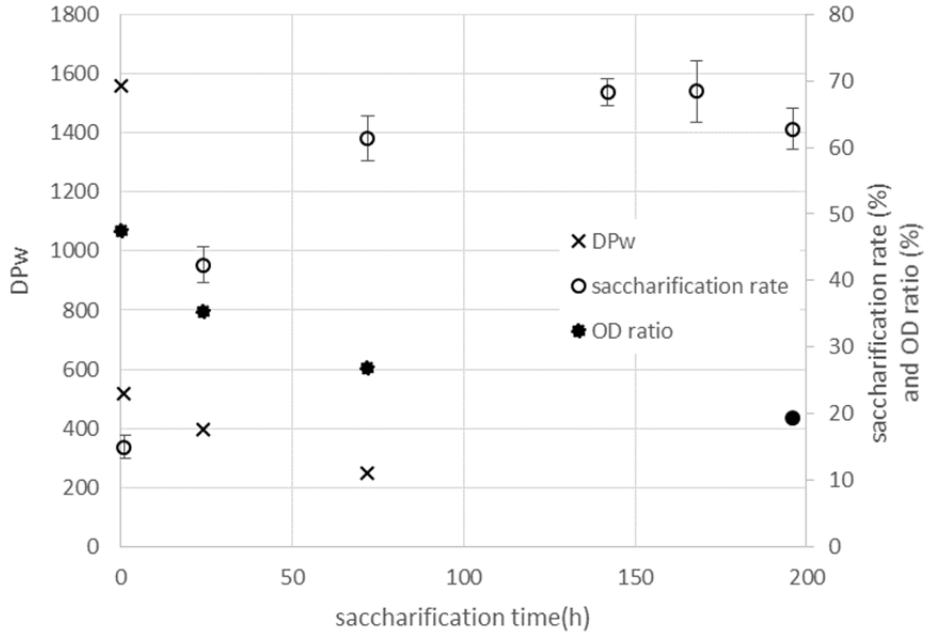

Figure 2. 2 Saccharification rates, weight-averaged degrees of polymerization (DP_ws), and OD ratios for bagasse cellulose hydrolyzed using Accellerase1500. Open circles are saccharification rates, filled circles are OD ratios, and crosses are DP_ws.

2.3.2 Weight-averaged DP

The hydrolysis of cellulose by endoglucanase causes the weight-averaged DP (DP_w) to decrease rapidly (Horikawa et al. 2016). This is because endoglucanase cuts cellulose chains at random points in amorphous regions. In this study, the DP_w decreased rapidly in the first hour of incubation but the saccharification rate remained below 20% at that time (Fig. 2.2). This indicated that the cellulose chains had been cut into shorter molecules but that not much glucose was produced at the beginning of the hydrolysis process. The DP_w then slowly decreased but the saccharification rate increased rapidly, mainly through the actions of two cellobiohydrolases. OD ration in Fig. 2.2 will be mentioned in 2.3.5.

2.3.3 TEM

The cellulose microfibrils before saccharification had been performed were more than several micrometers long. The ends of the microfibrils could not be seen, so

it was not possible to determine the actual lengths of the microfibrils (Fig. 2.3a). The microfibrils had become drastically shorter after 1 h of saccharification (Fig. 2.3b), and the microfibrils were slightly shorter still after 196 h of saccharification (Fig. 2.3c). The lengths and widths of the microfibrils were determined using Image J software. The microfibrils became shorter during the first phase of the saccharification process, which lasted ~24 h. The saccharification process caused the cellulose microfibrils to become both shorter and narrower (Fig. 2.4). This agreed with the decrease in DP_w. The saccharification residues became aggregated (Fig. 2.3b and 2.3c). Large cellulose aggregates were also visible under TEM when the saccharification process had been occurring for 24 h.

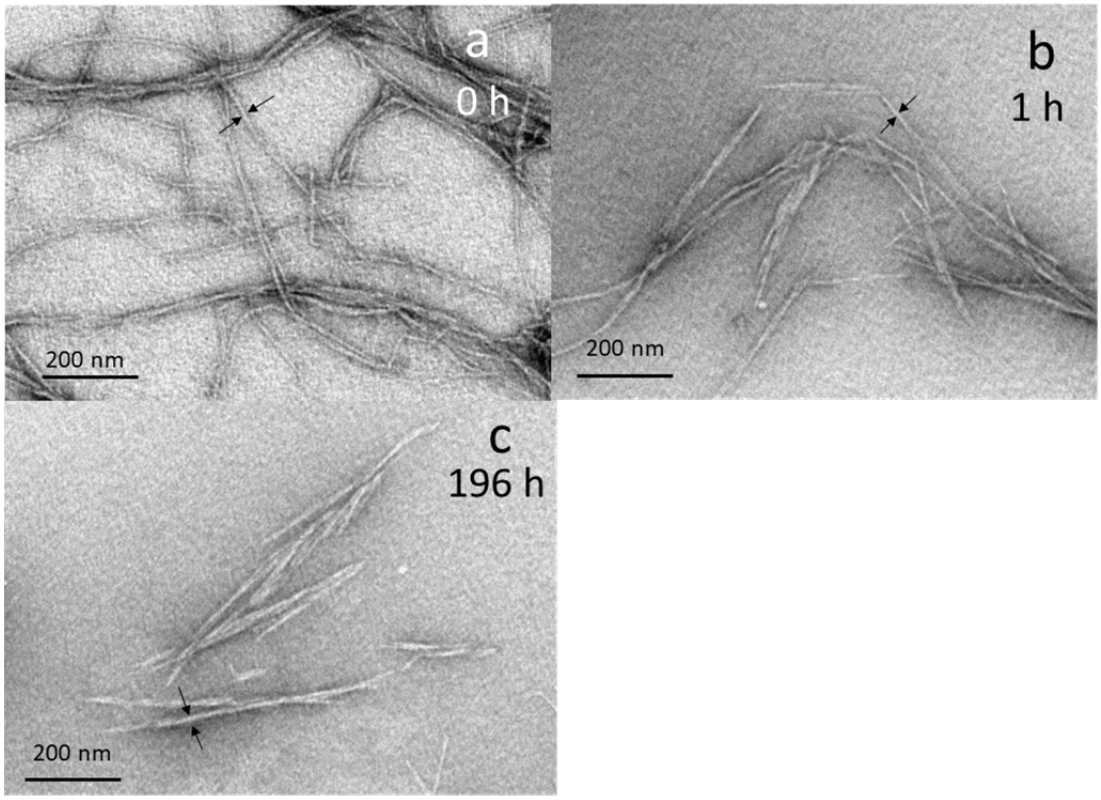

Figure 2.3 Transmission electron microscopy images of negative stained bagasse cellulose a) before saccharification, b) after saccharification for 1 h, and c) after saccharification for 196 h. Each pair of arrows indicates the measured width.

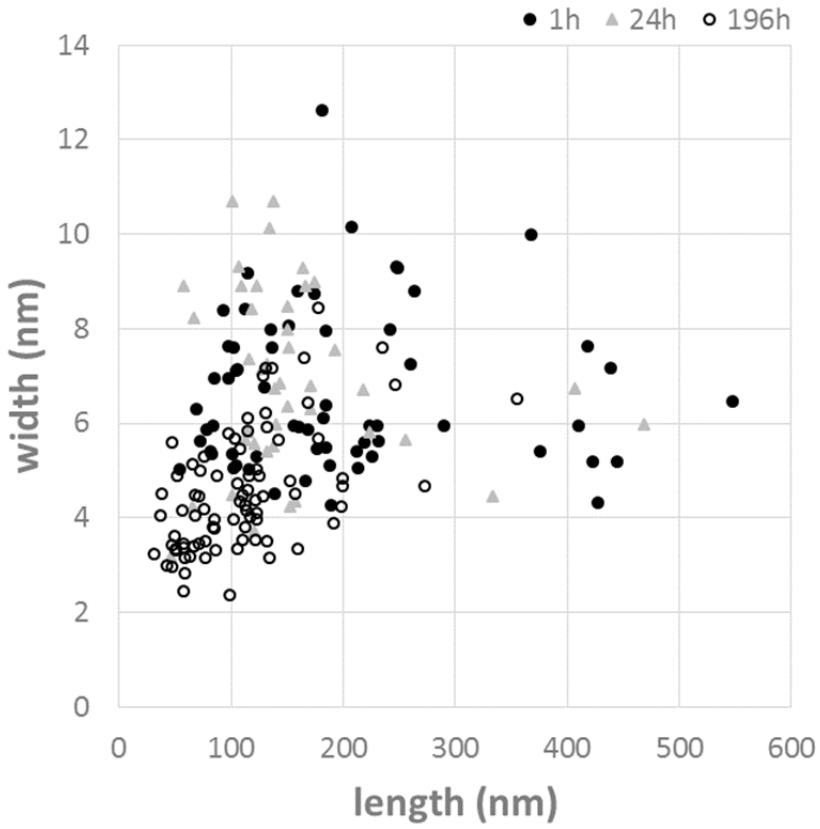

Figure 2.4 Lengths and widths of saccharified cellulose residues. Filled black circles are data for cellulose saccharified for 1 h, filled gray circles are data for cellulose saccharified for 24 h, and open circles are data for cellulose saccharified for 196 h.

2.3.4 SAXS analysis

Structural changes in the cellulose caused by cellulase were identified by performing SAXS analysis of an aqueous sample. The cellulose residue after 142 h of saccharification was subjected to SAXS analysis. The saccharification rate had reached a maximum at 142 h, as shown in Fig. 2.2, so it was reasonable to use the residue after 142 h of saccharification as a substitute for the residue after 196 h of saccharification. The *q*-region of the SAXS signal was limited, so the author qualitatively interpreted the *q*–*I* curve shown in Fig. 2.5. The SAXS data were prepared by subtracting the SAXS profile of pure water from the SAXS profile of the aqueous residue sample.

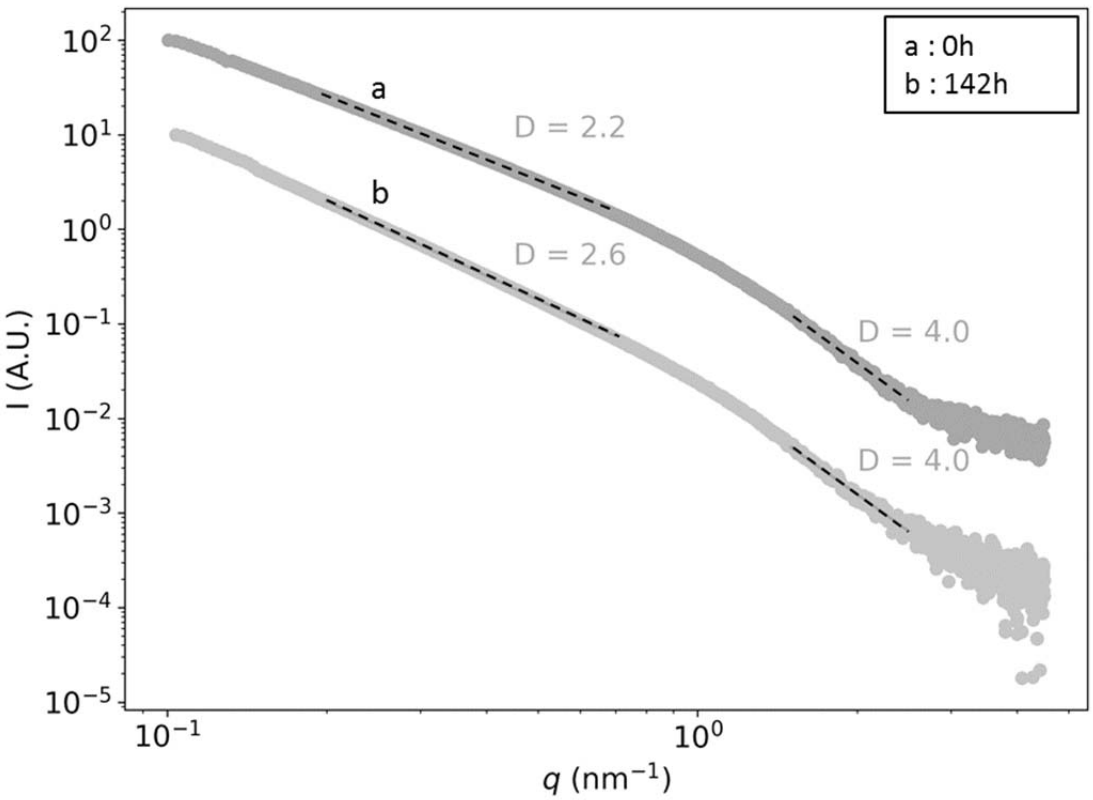

Figure 2.5 Small angle X-ray scattering data shown as a double-logarithmic *q*–*I* plot for nano-fibrillated cellulose samples 0 and 142 h after cellulase hydrolysis started. a) Before saccharification. b) After saccharification for 142 h. Circles are measured data. Straight lines were fitted to the results using the power law $I(q) \propto q^{-D}$, and the *D* values obtained are shown.

A shoulder feature was found at around q = 1 nm^{-1} for cellulose both before and after treatment with cellulase. This could be explained by the presence of highly dispersed cellulose microfibrils with sharp interfaces with the solvent, as was found in previous studies (Mao et al. 2017; Schmitt et al. 2018). The higher-q region of this shoulder feature (1.5–2.5 nm^{-1}) was successfully fitted using the power law in the form $I(q) \propto q^{-D}$, where D = 4 for both samples, as shown in Fig. 2.5. This could be interpreted as indicating that scattering occurred at the cellulose interface with a surface fractal dimension of two (i.e., 6 – D). The cellulose interface (i.e., the cellulose microfibril surface) was assumed to be, on average, smooth before and after hydrolysis by cellulase. The lack of change in this parameter indicated that the surfaces of the cellulose microfibrils that remained after 142 h of cellulase hydrolysis were as smooth as the surfaces of the microfibrils before they were hydrolyzed. A similar study with more frequent sampling times will need to be performed to allow a more detailed interpretation to be made.

Another important feature of the SAXS profile was monotonic scattering decay in the range q = 0.2–0.7 nm^{-1}. This q-region was fitted to the power law $I(q) \propto q^{-D}$, and the values of D for the 0 and 142 h hydrolysis time samples were 2.2 and 2.6, respectively. Perfectly dispersed plant cellulose microfibrils would be expected to exhibit scattering decay along a q^{-1} asymptote in this q-region, as found in a previous study (Schmitt et al. 2018). The D values used in this study were >2, clearly indicating that the cellulose microfibrils were aggregated rather than dispersed. Hydrolysis by cellulase clearly increased the D value in this q-region. The increase in the D value indicated that the structures at the size corresponding to the q values became denser. This change in the SAXS profile probably indicated that cellulose microfibrils were more densely packed after hydrolysis by cellulase than before. This agreed with the conclusion drawn from the TEM images that cellulase hydrolysis removed dispersed long microfibrils and caused cellulose microfibrils with similar lengths (~200 nm) to form aggregates (Fig. 2.3a and 2.3c).

2.3.5 IR spectra of deuterated bagasse cellulose

Cellulose has numerous hydroxyl groups that form intracellular and intercellular hydrogen bonds with each other. However, free hydroxyl groups are

exposed on cellulose microfibril surfaces, and the hydrogen atoms in these groups can easily be replaced with deuterium when the cellulose is stored in deuterium oxide. It is difficult to acquire an IR spectrum of deuterated cellulose because the OD groups in deuterated cellulose easily return to being OH groups when the system is exposed to H_2O in the air. IR spectra of deuterated cellulose in deuterium oxide vapor have been acquired (Tsuboi 1957; Hofstetter et al. 2006). In this study, a cellulose suspension in deuterium oxide was applied to an ATR prism and a spectrum was acquired while the cellulose was enveloped in a dry nitrogen atmosphere. No absorbance was found at ~2500 cm^{-1} (absorbance by OD) before the cellulose was deuterated (Fig. 2.6).

However, the spectrum of the deuterated cellulose both before and after 196 h of saccharification contained an OD absorption peak (Fig. 2.6). As more saccharification occurred, the OD ratio decreased from >40% to <20% (Fig. 2.2). It has previously been found that cellulase binds to hydrophobic planes of cellulose and then

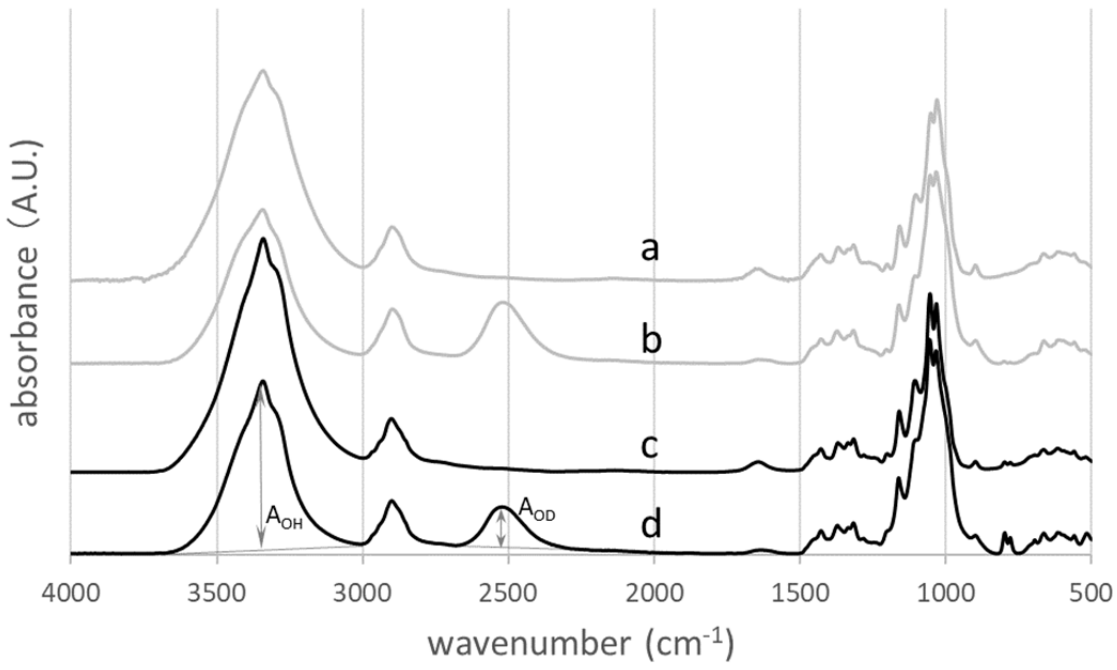

Figure 2.6 Infra-red spectra of bagasse cellulose a) before hydrolysis and before deuteration, b) before hydrolysis and after deuteration, c) after hydrolysis for 196 h and before deuteration, and d) after hydrolysis for 196 h and after deuteration.

starts to hydrolyze the cellulose (Lehtio et al. 2003; Liu et al. 2011). The exposed hydroxyl group ratio decreased and more hydrophobic planes became exposed as cellulose I was hydrolyzed from the hydrophobic planes (Fig. 2.7).

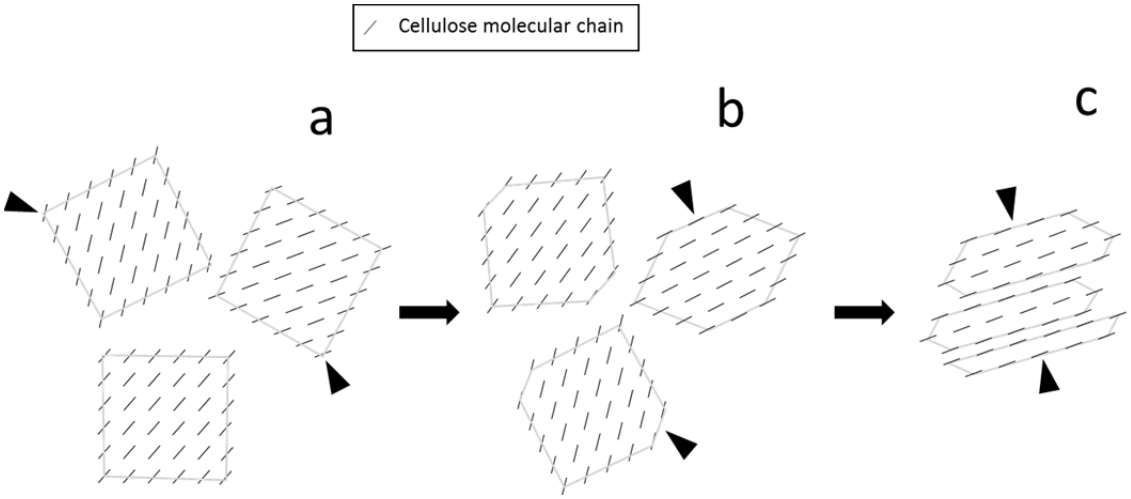

Figure 2.7 Cellulose microfibril cross-section during saccharification a) before saccharification, b) after saccharification for 1 h, and c) after the saccharification rate reached its limit. Arrowheads indicate hydrophobic planes.

Cellulose I has two crystal forms, cellulose I_α and cellulose I_β (Atalla and Vanderhart 1984). Sugarcane is a higher plant that contains only cellulose I_β. The cellulose microfibrils are synthesized by the cellulose synthase enzyme complex visualized in the plasma membrane as rosettes. It has been proposed that the microfibril consists of 36 molecular chains (Delmer 1999). In recent years, various models (e.g. 18 molecular chains, 24 molecular chains) have been proposed by some researchers (Fernandes et al. 2011; Oehme et al. 2015; Kubicki et al. 2018). In this study, theoretical OD ratios were calculated for the conventional 36 molecular chains model. A cellulose microfibril consisting of 36 molecules will have the cross-section before saccharification shown in Fig. 2.7a. The saccharification rate was 15%, and the microfibrils became shorter after an hour of saccharification. The cellulose molecules

would be hydrolyzed from two hydrophobic planes, and the cross-sections would have the structures shown in Fig. 2.7b. The microfibrils were then saccharified further and the hydrophobic plane areas increased. Once the saccharification reached the limit, the short microfibrils aggregated through hydrophobic effects (Fig. 2.7c). This was consistent with the cellulose residue aggregation observed by TEM. The ratio of hydroxyl groups exposed on the outsides of the microfibrils was calculated (Fig. 2.8).

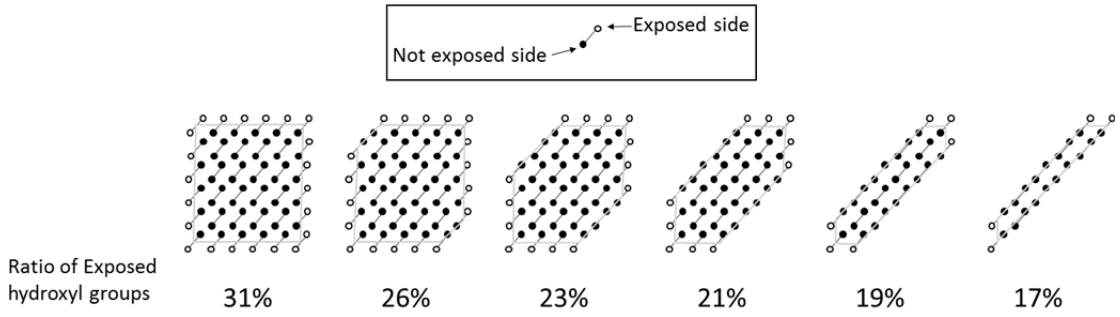

Figure 2. 8 Cellulose microfibril cross-section with the exposed hydroxyl group ratio. Open circles are exposed sides of cellulose molecular chains, and filled circles are non-exposed sides of cellulose molecular chains.

The ratio before saccharification was 31%, although the ratio of deuterated hydroxyl groups determined from the IR spectrum was 47%. The discrepancy was caused by microfibrils having some disordered parts with hydroxyl groups that could be deuterated. As saccharification progressed, the ratio of exposed hydroxyl groups gradually decreased to ~20%, as did the ratio of deuterated hydroxyl groups (Fig. 2.8). The accessibility of the cellulose to cellulase decreased as the hydrophilicity decreased and aggregation increased, and this explained the cellulose residues becoming more difficult to hydrolyze. Cellulose III_I is more easily hydrolyzed than cellulose I, and does not have a saccharification limit (Horikawa et al. 2013). This is because cellulose III_I has wider moderately hydrophobic planes that enzymes can become attached to and hydrolyze (Igarashi et al. 2011). Moderately hydrophobic planes also have free hydroxyl groups on their surfaces (Fig. 2.9).

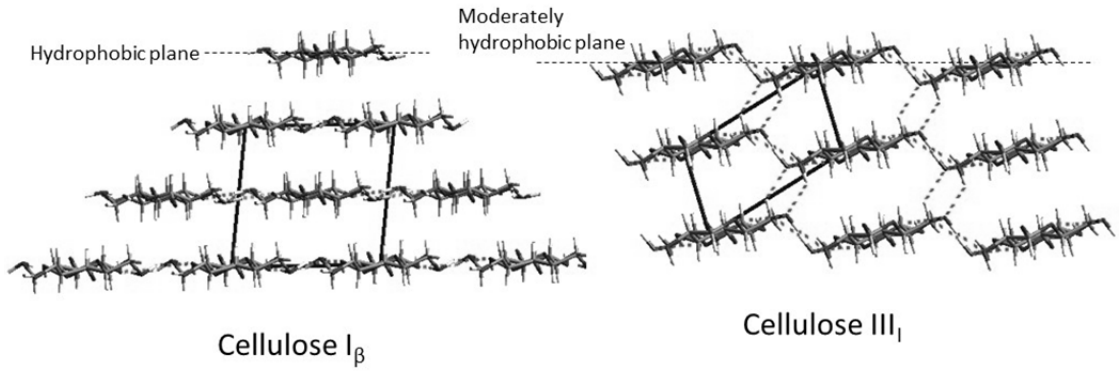

Figure 2.9 Crystal structures of cellulose I_β and cellulose III_I (modified from The Cellulose Microfibril and its Polymorphs (Sugiyama and Horikawa 2008). a) Cross-section of cellulose I. b) Cross-section of cellulose III_I.

The ratio of free hydroxyl groups on moderately hydrophobic plane surfaces will probably not decrease even though enzymes will hydrolyze cellulose III_I along its planes. This is a distinctive structure in cellulose III_I that is not present in cellulose I.

2.4 Conclusions

Sugarcane bagasse cellulose microfibrils decreased in length to ~200 nm in the early stages of saccharification and also gradually became narrower. Cellulose I was hydrolyzed from the hydrophobic planes, and the hydrophilicity decreased as saccharification proceeded. Aggregation of the saccharification residues was observed by TEM. This was supported by SAXS analysis results, including of a complete cellulose suspension. Aggregation was caused by hydrophobic effects derived from exposed wide hydrophobic planes. The results indicated that exposure of hydrophobic planes and hydrophilicity are required for enzymatic saccharification to occur. Decreasing hydrophilicity during saccharification is probably one of the reasons enzymatic saccharification of cellulose is limited.

2.5 List of abbreviations

ATR	attenuated total reflection
DP	degree of polymerization
DP_w	weight-averaged degree of polymerization
FT	Fourier-transform
IR	infra-red
SAXS	small angle X-ray scattering
TEM	transmission electron microscopy

2.6 References

Atalla RH, Vanderhart DL (1984) Native cellulose: A composite of two distinct crystalline forms. Science 223:283–285. https://doi.org/10.1126/science.223.4633.283

Atreya ME, Strobel KL, Clark DS (2016) Alleviating product inhibition in cellulase enzyme Cel7A. Biotechnol Bioeng 113:330–338. https://doi.org/10.1002/bit.25809

Delmer DP (1999) CELLULOSE BIOSYNTHESIS: Exciting times for a difficult field of study. Annu Rev Plant Physiol Plant Mol Biol 50:245–276. https://doi.org/10.1146/annurev.arplant.50.1.245

Fernandes AN, Thomas LH, Altaner CM, et al (2011) Nanostructure of cellulose microfibrils in spruce wood. Proc Natl Acad Sci 108:E1195–E1203. https://doi.org/10.1073/pnas.1108942108

Grethlein HE, Converse AO (1991) Common aspects of acid prehydrolysis and steam explosion for pretreating wood. Bioresour Technol 36:77–82. https://doi.org/10.1016/0960-8524(91)90101-O

Gunjikar TP, Sawant SB, Joshi JB (2001) Shear deactivation of cellulase, exoglucanase, endoglucanase, and beta-glucosidase in a mechanically agitated reactor. Biotechnol Prog 17:1166–1168. https://doi.org/10.1021/bp010114u

Hallac BB, Sannigrahi P, Pu Y, et al (2009) Biomass characterization of *Buddleja davidii*: A potential feedstock for biofuel production. J Agric Food Chem 57:1275–1281. https://doi.org/10.1021/jf8030277

Hofstetter K, Hinterstoisser B, Salmén L (2006) Moisture uptake in native cellulose – the roles of different hydrogen bonds: a dynamic FT-IR study using deuterium exchange. Cellulose 13:131–145. https://doi.org/10.1007/s10570-006-9055-2

Horikawa Y, Imai T, Abe K, et al (2016) Assessment of endoglucanase activity by analyzing the degree of cellulose polymerization and high-throughput analysis by near-infrared spectroscopy. Cellulose 23:1565–1572. https://doi.org/10.1007/s10570-016-0927-9

Horikawa Y, Konakahara N, Imai T, et al (2013) The structural changes in crystalline cellulose and effects on enzymatic digestibility. Polym Degrad Stab 98:2351–2356. https://doi.org/10.1016/j.polymdegradstab.2013.08.004

Horikawa Y, Sugiyama J (2008) Accessibility and size of *Valonia* cellulose microfibril studied by combined deuteration/rehydrogenation and FTIR technique. Cellulose 15:419–424. https://doi.org/10.1007/s10570-007-9187-z

Igarashi K, Uchihashi T, Koivula A, et al (2011) Traffic jams reduce hydrolytic efficiency of cellulase on cellulose surface. Science 333:1279–1282. https://doi.org/10.1126/science.1208386

Imai T, Sun S, Horikawa Y, et al (2014) Functional reconstitution of cellulose synthase in *Escherichia coli*. Biomacromolecules 15:4206–4213. https://doi.org/10.1021/bm501217g

Kubicki JD, Yang H, Sawada D, et al (2018) The shape of native plant cellulose microfibrils. Sci Rep 8:1–8. https://doi.org/10.1038/s41598-018-32211-w

Lehtio J, Sugiyama J, Gustavsson M, et al (2003) The binding specificity and affinity determinants of family 1 and family 3 cellulose binding modules. Proc Natl Acad Sci 100:484–489. https://doi.org/10.1073/pnas.212651999

Liu Y-S, Baker JO, Zeng Y, et al (2011) Cellobiohydrolase hydrolyzes crystalline cellulose on hydrophobic faces. J Biol Chem 286:11195–11201. https://doi.org/10.1074/jbc.M110.216556

Lou H, Wang M, Lai H, et al (2013) Reducing non-productive adsorption of cellulase and enhancing enzymatic hydrolysis of lignocelluloses by noncovalent modification of lignin with lignosulfonate. Bioresour Technol 146:478–484. https://doi.org/10.1016/j.biortech.2013.07.115

Mao Y, Liu K, Zhan C, et al (2017) Characterization of nanocellulose using small-angle neutron, X-ray, and dynamic light scattering techniques. J Phys Chem B 121:1340–1351. https://doi.org/10.1021/acs.jpcb.6b11425

Nishiyama Y, Isogai A, Okano T, et al (1999) Intracrystalline deuteration of native cellulose. Macromolecules 32:2078–2081. https://doi.org/10.1021/ma981563m

Oehme DP, Downton MT, Doblin MS, et al (2015) Unique aspects of the structure and dynamics of elementary Iβ cellulose microfibrils revealed by computational simulations1[OPEN]. Plant Physiol 168:3–17. https://doi.org/10.1104/pp.114.254664

Palonen H, Tjerneld F, Zacchi G, Tenkanen M (2004) Adsorption of *Trichoderma reesei* CBH I and EG II and their catalytic domains on steam pretreated

softwood and isolated lignin. J Biotechnol 107:65–72. https://doi.org/10.1016/j.jbiotec.2003.09.011

Saini JK, Patel AK, Adsul M, Singhania RR (2016) Cellulase adsorption on lignin: A roadblock for economic hydrolysis of biomass. Renew Energy 98:29–42. https://doi.org/10.1016/j.renene.2016.03.089

Schmitt J, Calabrese V, Silva MA da, et al (2018) TEMPO-oxidised cellulose nanofibrils; probing the mechanisms of gelation via small angle X-ray scattering. Phys Chem Chem Phys 20:16012–16020. https://doi.org/10.1039/C8CP00355F

Tsuboi M (1957) Infrared spectrum and crystal structure of cellulose. J Polym Sci 25:159–171. https://doi.org/10.1002/pol.1957.1202510904

Wada M, Okano T, Sugiyama J (1997) Synchrotron-radiated X-ray and neutron diffraction study of native cellulose. Cellulose 4:221–232. https://doi.org/10.1023/A:1018435806488

Wise LE, Murphy M, D'Addieco AA (1946) Chlorite holocellulose, its fractionation and bearing on summative wood analysis and studies on the hemicelluloses. Pap Trade J 122:35–43

Chapter 3 Direct observation of cellulase penetration in oven-dried pulp by confocal laser scanning microscopy

3.1 Introduction

Bleached wood pulps mainly consist of cellulose and hemicellulose. So, the inhibition of saccharification by lignin is not an issue for the bleached pulps. However, drying pulps negatively influences saccharification (Nazhad et al. 1995; Duan et al. 2015). Water is removed by drying and new hydrogen bonds are produced between the cellulose microfibrils (Nazhad et al. 1995). As a result, fibers become stiff and this phenomenon is called “hornification”. It was also reported that during this process, besides hydrogen bonds, ester and ether bonds, two types of covalent bonds, produced new networks of microfibrils (Fernandes Diniz et al. 2004; Chen et al. 2011). Despite numerous studies investigating hornification, the mechanism of hornification is not yet revealed. Many researchers have reported that it is more difficult to hydrolyze dried pulp than never-dried (ND) pulp (Nonaka and Nakagawa 2010; Luo and Zhu 2011). One of the reasons that saccharification of wood pulp may be difficult is thought to be because of a lower accessibility of enzymes to cellulose. Evidence of the lower accessibility includes reports of the decrease of adsorbed dye (Esteghlalian et al. 2001) or enzyme on dried cellulose (Wang et al. 2012) and the decrease of pore size of dried pulp (Chen et al. 2011; Lovikka et al. 2016). Additionally, pores observed on the surface of ND kraft pulp fibers and dissolving pulp by scanning electron microscopy were lost after oven drying (Lovikka et al. 2016).

Another phenomenon, dislocation, is well-known to be a defect in plant fiber cells. Dislocations may be induced by mechanical action both before and after harvest. Dislocations are susceptible to hydrolysis by acids and enzymes (Ander et al. 2008).

To well understand the mechanism of the enzymatic hydrolysis, visualizations of interactions between enzymes and biomass have been tried by using fluorescently labeled enzymes. The real-time enzyme binding to pretreated hardwood with fluorescently labeled cellulases was observed using a confocal laser scanning microscope (CLSM). (Zhu et al. 2011). Fluorescently labeled Cel7A from *Trichoderma*

reesei was more observed on pretreated wood particles than untreated wood particles using CLSM (Luterbacher et al. 2015). CLSM has a high spatial resolution in depth and three-dimensional images can be obtained. In this study, the author observed in real-time the adsorption, desorption, and penetration of fluorescently labeled enzymes to softwood kraft pulp using CLSM in an effort to visually estimate the accessibility of the enzymes. Pulps of three different water contents were used. These are 1) never-dried (ND) pulp, 2) pressed (PR) pulp, the pulp made of ND pulp by passing through press rollers to remove excess water, and 3) oven-dried (ODr) pulp. Additionally, the hemicellulose distribution of the pulp was determined to clarify the relationship between hemicellulose content and dislocation.

3.2 Materials and methods

3.2.1 Pulps

Softwood oxygen bleached kraft pulp of three different water contents was produced by Oji Holdings Corporation (Tokyo, Japan). The water contents were 65 %, 50 %, 7 % for never-dried (ND) pulp, pressed (PR) pulp, and oven-dried (ODr) pulp at 105 °C for 18 h, respectively.

3.2.2 Measurement of pulp width

As mentioned above, there are various studies that suggest the pore size of pulp fiber decreases or pores are lost after drying. Theoretically, the width of pulp fiber should become smaller after drying. The width of pulp fibers before hydrolysis was measured. ND, PR, and ODr pulps were spread on a glass slide (Matsunami, Osaka, Japan). A few drops of water were added and the sample was covered with a cover slip (Matsunami). The samples were observed with an optical BX51 microscope (Olympus, Tokyo, Japan). Images were captured by cellSens software (Olympus). Softwood pulp consists of two types of tracheids, latewood and earlywood tracheids. The former is a thick-walled fiber, while the latter is a thin-walled fiber with many bordered-pits. Since the earlywood tracheid deteriorated too fast to be measured quantitatively, the author only focused on latewood tracheids for width measurement. One or two points from the

body part of a tracheid excluding tips and dislocations were measured by using ImageJ software (n= 100).

3.2.3 Enzymatic Hydrolysis

Each pulp sample (20 mg on a dry matter basis) was hydrolyzed in 2 mL of enzyme solution at 50 °C with shaking at 150 rpm. The enzyme solution consisted of Celluclast® 1.5L (batch number: CCN03130, Novozymes, Bagsværd, Denmark) and β-glucosidase from *Aspergillus niger* (Megazyme, Bray, Ireland). The enzyme was loaded at 20 mg/g of pulp for each enzyme in 100 mM acetate buffer (pH 5.0). The enzyme concentration was measured using the Quick Start™ Bradford protein assay (Bio-Rad, Hercules, USA) with a gamma-globulin standard. The liquid fractions were collected at 3, 25, and 44 h to measure the D-glucose yield by the CII Test Wako kit (Wako, Osaka, Japan). The residue after 25 h of hydrolysis was observed using an optical BX51 microscope. As a control, each pulp sample in 100 mM acetate buffer without enzymes was shaken at 150 rpm at 50 °C for 25 h. The pulp was observed using an optical BX51 microscope. The enzymatic hydrolysis test by labeled Celluclast® 1.5L was also done to check the enzyme activity.

3.2.4 Labeling of enzyme with fluorescence dye

The medium solution of Celluclast® 1.5L was replaced with 10 mM phosphate buffered saline (PBS, pH 7.2) using an ultrafiltration spin column Vivaspin2® (molecular weight cut off 10 kDa, GE Healthcare, Chicago, USA). The enzyme was labeled with Alexa Fluor® 546 (Invitrogen, Carlsbad, USA) (Fig. 3.1) in accordance with the manufacturer's instructions. Bio-Gel® P-4 Gel fine (Bio-Rad, wet bead size 45–90 μm, molecular weight exclusion limit > 4,000 Da) was used to separate the labeled enzyme from the free dye.

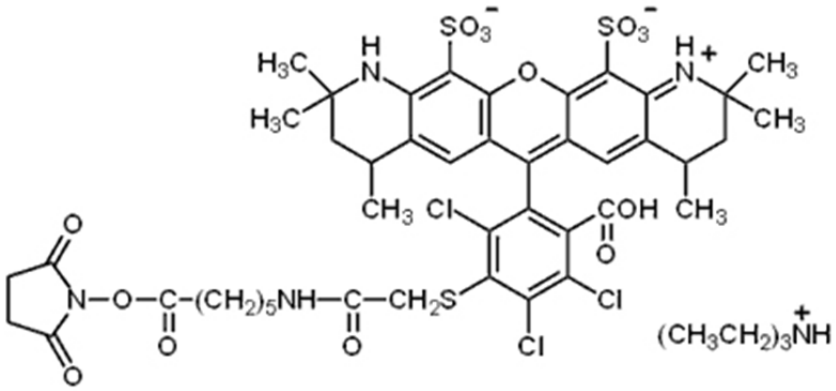

Figure 3.1 Alexa Fluor 546® molecule (cited from webpage of Thermo Fisher Scientific)

3.2.5 Observation of enzyme penetration to pulps

Each pulp (5 mg on a dry matter basis) was hydrolyzed in 0.5 mL of enzyme solution at 50 °C with shaking at 150 rpm. The enzyme solution consisted of non-labeled Celluclast® 1.5L, labeled Celluclast® 1.5L (Celluclast®-AF546) and β-glucosidase loaded at 10 mg/g of pulp, 10 mg/g of pulp, and 20 mg/g of pulp, respectively, in 100 mM acetate buffer (pH 5.0). A small portion of the pulps was removed from the reaction tube after 1, 4, and 25 h, mounted on a glass slide and covered with a cover slip. The cover slip was sealed with nail polish. The prepared specimens were observed with an Axiovert 100M confocal laser scanning microscope (CLSM) (Carl Zeiss, Oberkochen, Germany) at an excitation at 543 nm by a helium–neon laser. A x 40 objective lens (PLAN-Neofluar, NA=0.75) and PMT detector were used in this study. The emitted light was passed through a dichroic mirror (>545 nm), an emission long-pass filter (>560 nm), and a pin hole (125 μm). Z-stacks with a step size of 1 μm from the upper surface to the bottom surface were obtained with 512×512 pixels in each two-dimensional image acquired by LSM5Pascal (Carl Zeiss) software. Three-dimensional reconstruction was carried out by using ImageJ software.

3.2.6 Immunofluorescence microscopy for hemicellulose detection

After dehydration through a graded ethanol series, ND and ODr pulps were embedded in LR-white resin. Thin sections (2 μm) were prepared from the embedded blocks and mounted on cover slips. After treatment with PBS for 15 min, sections were suspended in blocking buffer (PBS buffer containing 1 % bovine serum albumin, 1 % blocking reagent (Sigma-Aldrich, St. Louis, USA)) for 30 min at room temperature. Thereafter, sections were incubated with LM11, a monoclonal antibody to xylan/arabinoxylan (Plant Probes, Leeds, UK; 1:20 dilution in blocking buffer) or monoclonal antibody to (1→4)- β-mannan and galacto-(1→4)- β-mannan (Biosupplies, Victoria, Australia; 1:20 dilution in blocking buffer) for 2 days at 4 °C. After washing three times with PBS buffer for 10 min each, the sections were incubated with anti-rat IgM Alexa Fluor® 488 (Invitrogen; 1:20 dilution in PBS buffer) or anti-mouse IgG Alexa Fluor® 488 (Invitrogen; 1:20 dilution in PBS buffer), respectively, for 2 h at 35 °C. After washing three times with PBS buffer for 10 min each, the sections were examined under an inverted fluorescent microscope (IX71, Olympus, Tokyo, Japan) with the filter set U-MWIB3 (Olympus) and a polarized microscope. No fluorescence was detected on the sections treated in the absence of primary antibody under the same conditions.

3.3 Results and discussion

3.3.1 Optical microscopic observation of pulp

Fig. 3.2 a–c shows the optical microscopic images of pulp fiber before hydrolysis. There are some parts like nodes or kinks (arrow heads) on the fibers. These parts are called dislocations and represent areas where the structure of the cell wall changes (Clarke et al. 2011). Dislocations, also called slip planes, are widely known in the pulp and paper field. From our results, dislocations existed not only in ODr pulp but also in PR pulp and ND pulp before enzymatic hydrolysis. Therefore, the dislocations were caused neither by hydrolysis nor by the drying process. It seemed that ODr pulp fibers became narrower than ND pulp fibers.

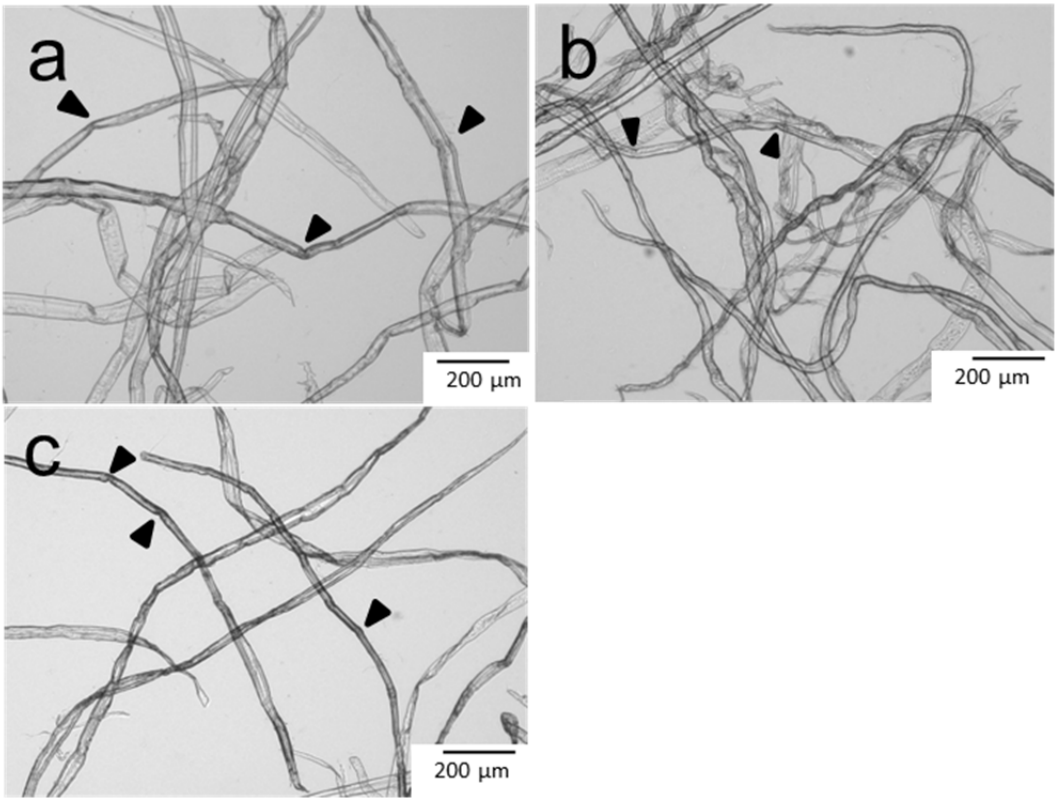

Figure 3.2 Optical microscopic images of pulp. Never-dried (ND) pulp (a), pressed (PR) pulp (b), and oven-dried (ODr) pulp (c). Many dislocations are observed (arrow heads).

3.3.2 Measurement of the width of pulp fibers

The width and a histogram of the width distribution of latewood tracheids are represented in Fig. 3.3a and 3.3b, respectively. While both ND and PR pulp had a maximum peak in the range of 25-30 μm, ODr pulp had a maximum peak in the range of 20-25 μm. The statistical data of the width are shown in Table 1. The average width decreased in the order of ND, PR, and ODr. The average width of ODr pulp was 77 % that of ND pulp. The width of the latewood tracheid was confirmed to have decreased because the water between the cellulose microfibrils in the cell wall was removed during the drying process.

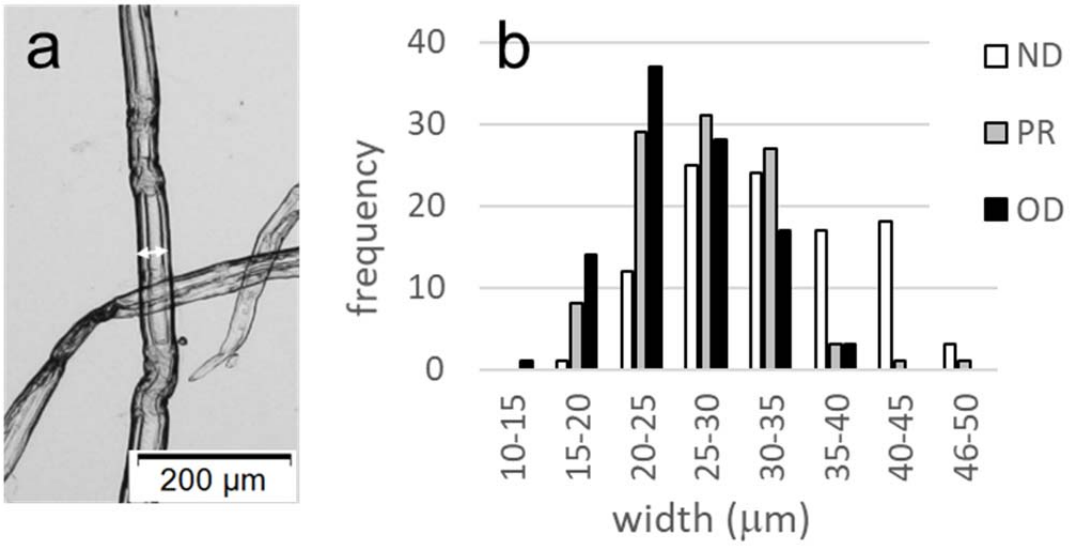

Figure 3.3 Measurement of the width of a latewood tracheid (a) microscopic image of never-dried (ND) pulp. Two direction arrows indicate the width. (b) Histogram of the width

Table 3.1 The width of latewood tracheids

	ND	**PR**	**ODr**
Average width (µm)	**32.8**	**27.1**	**25.2**
Standard deviation (µm)	**6.9**	**5.3**	**4.9**
Minimum width (µm)	**18.6**	**16.4**	**14.8**
Maximum width (µm)	**46.0**	**45.4**	**38.9**

n = 100 (ND, PR, and ODr); ND (never-dried); PR (pressed); ODr (oven-dried)

3.3.3 Enzymatic Hydrolysis

The saccharification rate of ND pulp was reconfirmed to be the highest followed by PR pulp and ODr pulp (Fig. 3.4). After 3 h of hydrolysis, the saccharification rate of ND pulp was already twice of that of ODr pulp. After 44 h, although more than 70 % of the cellulose of ND pulp was hydrolyzed, less than 40 % of

that of ODr pulp was hydrolyzed. After 25 h of hydrolysis, the residue was observed using an optical microscope.

ND pulp fibers were shortened to several hundred μm, the cell wall became thinner (Fig. 3.5a) and the cracks were hydrolyzed (Fig. 3.5a'). The fibers in the PR

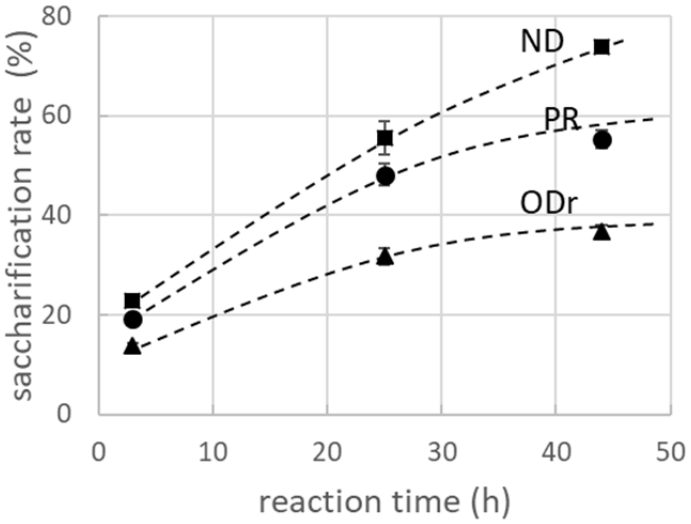

Figure 3.4 Saccharification rate of pulp by Celluclast® 1.5L and β-glucosidase

The error bars indicate the standard deviations of the measured values. Square: ND pulp, circle: PR pulp, triangle: ODr pulp.

pulp were generally shortened to several hundred μm and some were able to maintain the cell wall thickness (Fig. 3.5b). The cell walls of the ODr pulp fibers remained thick and some were more than 1 mm long. The microscope observations also supported the idea that ODr pulp is more difficult to hydrolyze than ND and PR pulps. Such morphological changes were never observed in any pulps without enzyme treatment. Numerous dislocations of ODr pulp fiber were in the middle of being cut (Fig. 3.5c). It was already reported that the susceptibility of dislocation to HCl and enzymes is high (Ander et al. 2008) and that pulp fibers cleaved especially in dislocations by enzymes (Ander et al. 2008; Clarke et al. 2011). Thus, it is assumed that amorphous cellulose is dominant in dislocation. In this study, it was observed pulp fibers were cut in areas of dislocation. However, there is a report that the existence of crystalline cellulose in areas of dislocation was deduced from a birefringence with a polarizing microscope

(Thygesen et al. 2011). In our study, earlywood tracheids with thin cell walls were easily hydrolyzed even in ODr pulp (Fig. 3.5c), so the major residues of the enzymatic hydrolysis were latewood tracheids with thick cell walls (Fig.3.5a–c). The author concluded the difficulty of hydrolysis of the latewood tracheids was one of the causes of the low saccharification. The author selectively observed latewood tracheids in the following observation of the penetration of cellulase.

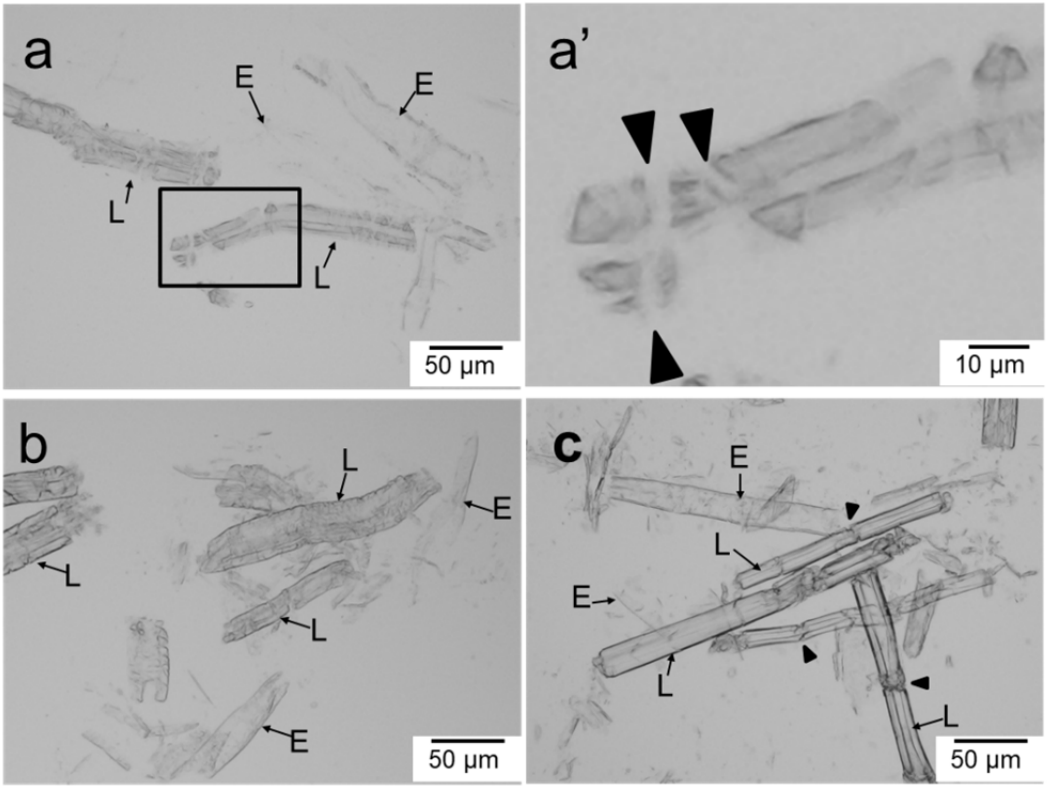

Figure 3.5 Optical microscopic images of residues of never-dried pulp (a), pressed pulp (b), and oven-dried pulp (c) hydrolyzed for 25 h by Celluclast® 1.5L and β-glucosidase. Boxed area in (a) is enlarged in (a'). Large arrow heads indicate hydrolyzed cracks (a') and small ones indicate the parts that are cut through (c). E and L indicate an earlywood tracheid and a latewood tracheid respectively.

3.3.4 Observation of the penetration of cellulase

The residues of pulps hydrolyzed by Celluclast®-AF546 and β-glucosidase for 1, 4, and 25 h were observed with a CLSM (Fig. 3.6). All images represent a center plane of a z-stack and the red pseudo-color is the fluorescence from the Alexa Fluor® 546

conjugated with Celluclast® 1.5L. It was reported that an over-labeling of fluorescence dye caused a reduction of enzymatic activities (Moran-Mirabal et al. 2009). Although the enzymatic activity of labeled Celluclast® 1.5L was reduced to 80 % of that of non-labeled Celluclast® 1.5L, the activity was enough to observe the behavior of enzymes by microscopy in this study. After hydrolysis for 1 h, cellulases were observed on the outer surfaces and cracks of the cell walls of the ND tracheid. On the inner surfaces, there were a small amount of cellulases that were considered to enter from the cracks (Fig. 3.6a). Additionally, many cellulases were observed on the dislocations (Fig. 3.6a insert). Cross-section images reconstructed from the z-stacks are shown in Fig. 3.7. The adsorption of enzymes to the surface and cracks and the penetration to the dislocation of the ND tracheid were clearly shown (Fig. 3.7a). Enzymes were adsorbed to the outer surface of the ODr tracheid and they penetrated only the cell walls of the dislocations (Fig. 3.6c, 3.7c). Thygesen et al. (2011) observed the specific adsorption of endoglucanase to dislocations. In this study, the author confirmed that cellulases were preferentially adsorbed to these sites. There was no large difference among the three types of pulp up to 1 h. After 4 h of hydrolysis, although cellulases penetrated the cell walls of the ND tracheid from every direction, that is, dislocations, outer surfaces, inner surfaces and cracks (Fig. 3.6d), they were particularly observed on the outer surfaces and dislocations of the ODr tracheids (Fig. 3.6f). For PR pulp, cellulases were observed in the inside of the cell walls of some of the tracheids and on the outer surfaces and dislocations of others (Fig. 3.6e). After 25 h of hydrolysis, almost all of the ND, PR, and ODr tracheids were shortened to several hundred μm (Fig. 3.6g–3.6i).

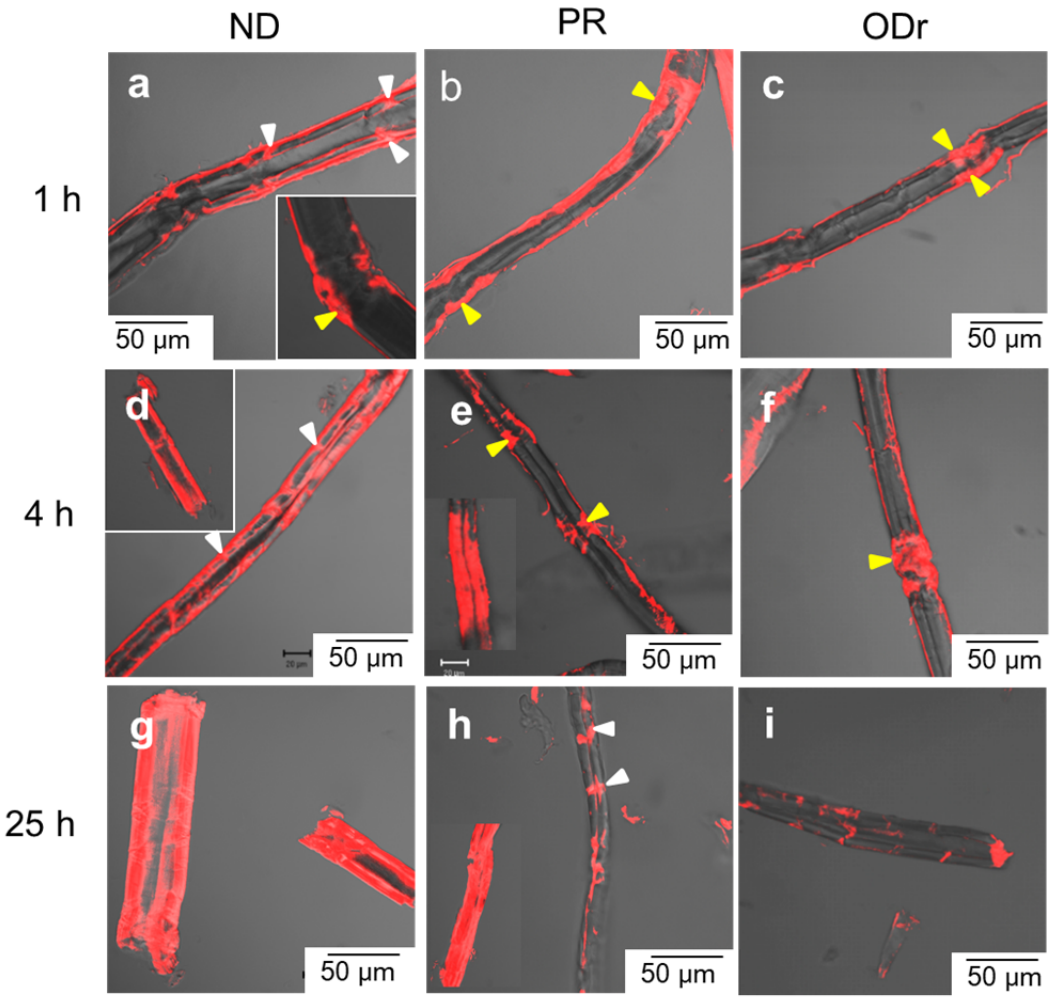

Figure 3.6 Confocal laser scanning microscopic images of residues of never-dried pulp (a, d, g), pressed pulp (b, e, h) and oven-dried pulp (c, f, i) hydrolyzed for 1 h (a–c), 4 h (d–f), and 25 h (g–i) by Celluclast®-AF546 and β-glucosidase. The red pseudo-color is the fluorescence of Alexa Fluor® 546 conjugated with Celluclast®1.5L. White arrows indicate cracks that cellulases enter. Yellow arrows indicate dislocations that cellulases penetrate.

A much higher amount of cellulases penetrated the inside of the cell walls of the ND tracheid (Fig. 3.6g, 3.7b). Although cellulases were only minimally observed in the inside of the cell walls of the ODr tracheid, they were on both ends and cracks of the ODr tracheid (Fig. 3.6i, 3.7d). Cellulases were observed in the inside of the cell walls of some of the PR tracheid and both ends and cracks of others (Fig. 3.6h). From these observations it can be concluded that cellulases hydrolyze cellulose in dislocations and remain there (on the ends of short pulps and cracks) without penetrating the inside of

the cell walls of the ODr tracheid. It is not clear what is keeping enzymes at dislocations. It might be a kind of traffic jams, a state of congested enzymes occurred at a fine split end of a tracheid wall.

As a result, the saccharification of the ODr pulp did not proceed. The cell walls of the ND tracheid became thinner in addition to becoming shorter because the cellulases penetrated the inside of the cell walls. Cellulases penetrated the whole cell walls of some PR tracheids and were adsorbed only on the surface and the dislocations of other PR tracheids. In other words, the hornification heterogeneously caused in PR tracheids. This is because of the unevenness of removal of water by press rollers.

Even after oven drying, cellulases can penetrate the cell wall in dislocations. This means that there are pores large enough for enzymes to enter on the cell wall of dislocations of ODr tracheids. In other words, hornification process does not “close” the dislocations completely and thus cellulases are still able to enter despite the shrinking hollow space in dislocations, which leads to the complete disruption of a tracheid by enzymes as observed in Fig. 3.6i and Fig. 3.7d. Though it is still speculative, according to the size of enzymes reported in the literatures (Abuja et al. 1988a, b, 1993; Lee and Brown 1997), the hollow size of the tracheid dislocations that permits enzyme intrusion could be estimated larger than at least 5-10 nm.

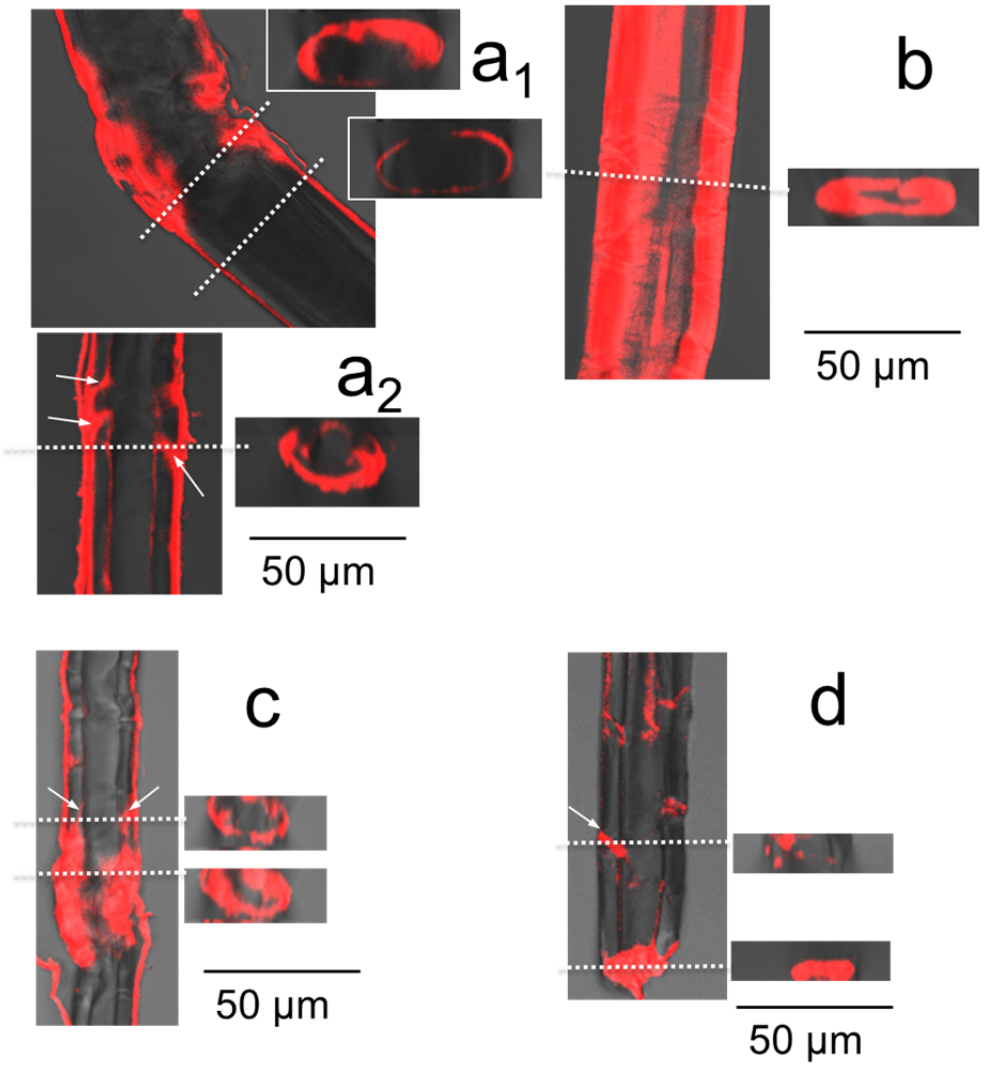

Figure 3.7 Typical confocal microscope images and the corresponding reconstructed cross-sectional views at the position indicated by the dashed lines. ND pulp, saccharified for 1 h (a_1, a_2), 25 h (b). ODr pulp, saccharified for 1 h (c), 25 h (d). The red pseudo-color is the fluorescence of Alexa Fluor®546 conjugated with Celluclast®1.5L. Arrows indicate cracks. Enzymes were always observed at the dislocations and cracks both in ND pulp and ODr pulp. At prolonged duration, enzymes were more penetrated into the whole part of ND pulp (b), while they are observed only along the cracks or on disrupted ends of ODr pulp (d).

3.3.5 Xylan and Mannan distribution on ND and ODr pulp

Hornification is caused by producing of some new bonds between cellulose microfibrils. The author assumed that the absence of hornification in dislocation was

attributed to the existence of some materials between cellulose microfibrils. Materials other than cellulose are hemicellulose and lignin in pulp fibers. It was previously reported that xylan was observed in the dislocations of eucalyptus soda pulp by the method of immunolabeling microscopy (Tamminen et al. 2018). However, the large antibody employed in this study did not penetrate into the cell wall, and thus the observations were limited to the fiber surface. Instead, the accessibility of xylan in kinks and dislocations was discussed rather than its distribution. In our study, longitudinal sections were examined to observe the distribution of hemicellulose in the fiber cell wall. The author tried to observe mannan and xylan by the method of immunolabeling microscopy because the primary softwood hemicelluloses are glucomannan, galacto-glucomannan, and arabino-glucuronoxylan. From a viewpoint of the hornification, PR fibers were not the state of intermediate between two types of pulp (ND and ODr) but found to be a mixture of representative ND and ODr fibers. Therefore, the author considered that the analysis of the ND and ODr fibers was enough to characterize the hornification process in this study.

Immunolabeling of mannan and xylan was primarily detected on dislocations of both ND and ODr pulp fibers (Fig. 3.8). Hornification is more remarkably caused by drying after removal of hemicellulose than before removal of hemicellulose (Oksanen et al. 1997; Rebuzzi and Evtuguin 2005). The hemicellulose between the cellulose microfibrils seems to have an important role to prevent hornification. Longitudinally uneven distribution of hemicellulose in a tracheid before pulping has not been presented to the best of our knowledge. Therefore, it is assumed that pulp fibers have some parts where hemicellulose was more difficult to remove than other parts during pulping.

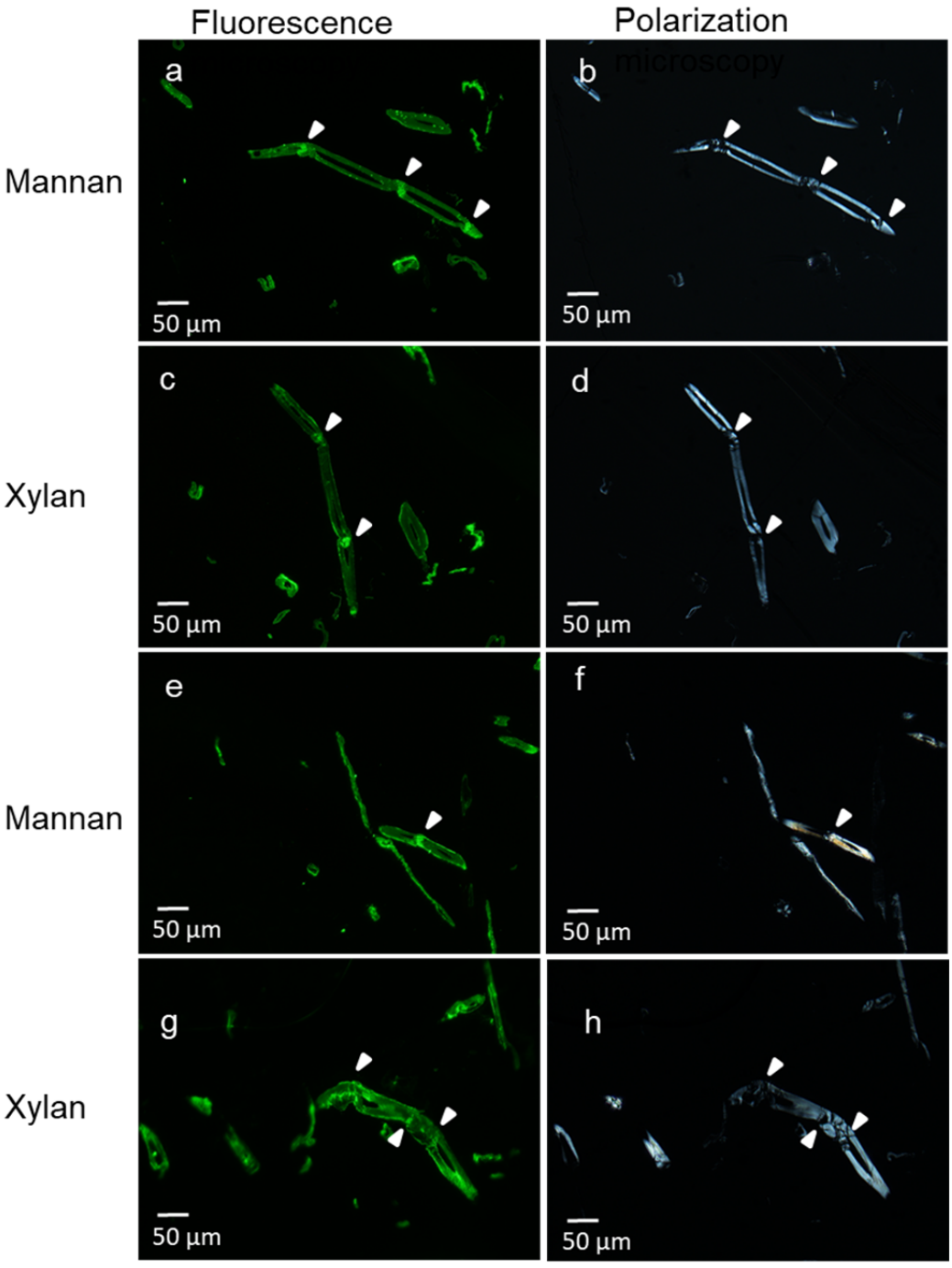

Figure 3.8 Confocal laser scanning microscopic (CLSM) and polarization microscopic (PM) images of immunofluorescence labeled pulp fibers. Never-dried (a–d); oven-dried (e–h); mannan distribution (a), (b), (e), and (f); xylan distribution (c), (d), (g), and (h). CLSM images in the left column and PM images in the right column.

3.4 Conclusion

The results from this study showed that cellulases could not penetrate the inside of cell walls and remained on dislocations and cracks on the latewood tracheids of ODr pulp. From this work and the reports of other researchers, the author conclude that the ODr tracheid does not have pores large enough on the surfaces for cellulases to enter. In contrast, it was observed that cellulases penetrated the latewood tracheids of ND pulp from both the outer and inner surfaces, dislocations and cracks. Even after oven drying, cellulases can penetrate the cell wall in dislocations and hydrolyze cellulose. This is because the areas of dislocation contain more hemicellulose than the other parts, which suppress the level of hornification.

3.5 List of abbreviations

CLSM	confocal laser scanning microscope
ND	never-dried
ODr	oven-dried
PR	pressed

3.6 References

Ander P, Hildén L, Daniel G (2008) Cleavage of softwood kraft pulp fibres by HCl and cellulases. BioResources 3:477-490–490. doi: 10.15376/biores.3.2.477-490

Abuja PM, Pilz I, Claeyssens M, Tomme P (1988a) Domain structure of cellobiohydrolase II as studied by small angle X-ray scattering: Close resemblance to cellobiohydrolase I. Biochem Biophys Res Commun 156:180–185. doi: 10.1016/S0006-291X(88)80821-0

Abuja PM, Schmuck M, Pilz I, et al (1988b) Structural and functional domains of cellobiohydrolase I from trichoderma reesei: A small angle X-ray scattering study of the intact enzyme and its core. Eur Biophys J 15:. doi: 10.1007/BF00254721

Abuja PP, Hayn M, Chen H, Esterbauer H (1993) The structure of endoglucanase I (*Trichoderma reesei)* in solution. In: Laggner P, Glatter O (eds) Trends in Colloid and Interface Science VII. Steinkopff, pp 181–181

Chen Y, Wan J, Huang M, et al (2011) Influence of drying temperature and duration on fiber properties of unbleached wheat straw pulp. Carbohydr Polym 85:759–764. doi: 10.1016/j.carbpol.2011.03.041

Clarke K, Li X, Li K (2011) The mechanism of fiber cutting during enzymatic hydrolysis of wood biomass. Biomass Bioenergy 35:3943–3950. doi: 10.1016/j.biombioe.2011.06.007

Duan C, Long Y, Li J, et al (2015) Changes of cellulose accessibility to cellulase due to fiber hornification and its impact on enzymatic viscosity control of dissolving pulp. Cellulose 22:2729–2736. doi: 10.1007/s10570-015-0636-9

Esteghlalian AR, Bilodeau M, Mansfield SD, Saddler JN (2001) Do enzymatic hydrolyzability and Simons' stain reflect the changes in the accessibility of lignocellulosic substrates to cellulase enzymes? Biotechnol Prog 17:1049–1054. doi: 10.1021/bp0101177

Fernandes Diniz JMB, Gil MH, Castro JAAM (2004) Hornification—its origin and interpretation in wood pulps. Wood Sci Technol 37:489–494. doi: 10.1007/s00226-003-0216-2

Lee HJ, Brown RM (1997) A comparative structural characterization of two cellobiohydrolases from *Trichoderma reesei*: a high resolution electron microscopy study. J Biotechnol 57:127–136. doi: 10.1016/S0168-1656(97)00111-9

Lovikka VA, Khanjani P, Väisänen S, et al (2016) Porosity of wood pulp fibers in the wet and highly open dry state. Microporous Mesoporous Mater 234:326–335. doi: 10.1016/j.micromeso.2016.07.032

Luo X, Zhu JY (2011) Effects of drying-induced fiber hornification on enzymatic saccharification of lignocelluloses. Enzyme Microb Technol 48:92–99. doi: 10.1016/j.enzmictec.2010.09.014

Luterbacher JS, Moran-Mirabal JM, Burkholder EW, Walker LP (2015) Modeling enzymatic hydrolysis of lignocellulosic substrates using fluorescent confocal microscopy II: Pretreated biomass. Biotechnol Bioeng 112:32–42. doi: 10.1002/bit.25328

Moran-Mirabal JM, Corgie SC, Bolewski JC, et al (2009) Labeling and purification of cellulose-binding proteins for high resolution fluorescence applications. Anal Chem 81:7981–7987. doi: 10.1021/ac901183b

Nazhad MM, Ramos LP, Paszner L, Saddler JN (1995) Structural constraints affecting the initial enzymatic hydrolysis of recycled paper. Enzyme Microb Technol 17:68–74. doi: 10.1016/0141-0229(94)00057-X

Nonaka H, Nakagawa A (2010) Comparison of soda and kraft cooking as a pretreatment method for enzymatic hydrolysis of softwood kignocellulosic materials. J Jpn Inst Energy 89:962–967. doi: 10.3775/jie.89.962

Oksanen T, Buchert J, Viikari L (1997) The Role of hemicelluloses in the hornification of bleached kraft pulps. Holzforschung 51:355–360

Rebuzzi F, Evtuguin DV (2005) Effect of glucuronoxylan on the hornification of *Eucalyptus globulus* bleached pulps. Macromol Symp 232:121–128. doi: 10.1002/masy.200551414

Tamminen T, Mikkelson A, Siika-aho M, et al (2018) Deposition of xylan isolated from *Pennisetum purpureum* on fibres of *Eucalyptus globulus* and characterisation

of the composition of the surface xylans by immunolabelling and enzymatic peeling. Holzforschung 72:915–922. doi: 10.1515/hf-2018-0002

Thygesen LG, Hidayat BJ, Johansen KS, Felby C (2011) Role of supramolecular cellulose structures in enzymatic hydrolysis of plant cell walls. J Ind Microbiol Biotechnol 38:975–983. doi: 10.1007/s10295-010-0870-y

Wang QQ, He Z, Zhu Z, et al (2012) Evaluations of cellulose accessibilities of lignocelluloses by solute exclusion and protein adsorption techniques. Biotechnol Bioeng 109:381–389. doi: 10.1002/bit.23330

Zhu P, Moran-Mirabal JM, Luterbacher JS, et al (2011) Observing *Thermobifida fusca* cellulase binding to pretreated wood particles using time-lapse confocal laser scanning microscopy. Cellulose 18:749–758. doi: 10.1007/s10570-011-9506-2

Chapter 4 Time-lapse enzyme visualization during sugarcane hydrolysis

4.1 Introduction

Among the numerous biomass materials, sugarcane has received significant attention at the industrial scale as one of the lignocelluloses for bioethanol production, particularly, with bagasse (fiber remaining after extracting sugarcane juice) being a focus of attention.

The native crude cellulase is composed of multiple enzyme components, each of which offers individual function and specific activity. The three main components are cellobiohydrolase (CBH), endoglucanase (EG), and β-glucosidase (BGL). Numerous reports have detailed the synergistic effect among these components (Henrissat et al. 1985; Beldman et al. 1988; Wood et al. 1989). Enzyme-substrate specificity has received significant attention that includes the development of visually observing their interactions. Classically, gold-labeled individual enzymes were visualized by electron microscopy (White and Brown 1981; Chanzy et al. 1984), and thereafter, cellulose-binding modules (CBMs) with fluorescein isothiocyanate (Jervis et al. 1997; Pinto et al. 2006) were observed. A single molecular motion of a green fluorescence protein-tagged CBM on a cellulose crystal of *Valonia ventricosa* was analyzed (Liu et al. 2010). Furthermore, a fluorescence resonance energy transfer technique (Wang et al. 2012) demonstrated that cellulases were located only a few nm from each other on the surface of a cellulose microfibril. More impressively, by high-speed atomic force microscopy, the running motion of CBH I particles, on a cellulose microfibril, from the cell wall of *Cladophora* sp. was directly visualized (Igarashi et al. 2009). The authors further investigated, and observed a type of “traffic jam” on the cellulose surface, and by theoretical analysis, elucidated a possible mechanism of the enzyme-substrate interaction (Igarashi et al. 2011).

As described above, the observation of ‘individual’ cellulase components has been successfully reported. Hitherto, however, such observations have not been directed

toward the visualization of each enzyme component in cellulase mixture working synergistically with real biomass tissue. Therefore, the focus of this study was to visualize the pattern of adsorption and desorption of each enzyme component acting on a section of sugarcane by fluorescence microscopy combined with a newly-developed image analysis technique.

Furthermore, this study also focused on xylanases as important enzymes for the hydrolysis of biomass. Two xylanases were selected for the visualization experiment: endoxylanase III (Xyn III) from *Trichoderma reesei*, well-known to be efficient and endoxylanase10 (Xyn10) from *Penicillium* sp., a recently found high-performance enzyme.

4.2 Materials and Methods

4.2.1 Enzyme preparation

The enzymes used in this study were CBH I (*Tr*Cel7A), CBH II (*Tr*Cel6A), EG I (*Tr*Cel7B), EG II (*Tr*Cel5A), EG IV (*Tr*Cel61A), Xyn III, β-xylosidase (*Tr*Xyl3A, BXL), BGL I, and Xyn10 (PspXyn10). CBH I, CBH II, EG I, EG II, EG IV, Xyn III and BXL were derived from the *T. reesei* strain PC-3-7 (Kawamori et al. 1986) and BGL I was derived from *Aspergillus aculeatus* (Kawaguchi et al. 1996). These eight enzymes were heterologously expressed in *A. oryzae* (Ozeki Co. Ltd., Hyogo, Japan) following the method reported by Kawai et al. (2012). Each enzyme was purified from the culture supernatant of *A. oryzae* cells by hydrophobic chromatography (TOYOPEARL®Butyl-650) followed by anion exchange chromatography (TOYOPEARL® DEAE-650).

To prepare Xyn10 from *Penicillium* sp., the *pspxyn10* gene was amplified from pUC-P*cbh1-pspxyn10-amdS* plasmid (Shibata et al. 2017) by a polymerase chain reaction and expressed in *A. oryzae* cells under the control of an improved *eno*A promoter (P*enoA*142f) (Tsuboi et al. 2005) that harbored 12 tandem repeats of the *cis*-acting element (region III) of the *agd*A promoter (Tsuboi et al. 2005). *A. oryzae* cells expressing the *pspxyn10* gene were cultured in a DP medium (2% dextrin hydrate, 1% peptone) containing 0.5% potassium dihydrogen phosphate, 0.05% magnesium

sulfate, 0.187% L-glutamic acid monosodium salt, and 0.003% L-methionine at 30 °C, 105 rpm for 3 days. After cultivation, the *A. oryzae* cells were removed by filtration (0.45 μm) and Xyn10 was purified as described above.

4.2.2 Enzyme labeling with a fluorescent dye

Herein, CBH I, CBH II, EG I, EG II, Xyn III, and Xyn10 were labeled with a fluorescent dye as theses enzymes are the main components of a wild-type of cellulase and have important functions.

Each enzyme was labeled with Alexa Fluor® 546 NHS Ester (Invitrogen, California, USA) in accordance with an attached instruction. The fluorescent molecule forms a covalent bond with a primary amine group in enzyme. Determination of the protein concentration was performed using a Quick Start™ Bradford protein assay (Bio-Rad, California, USA) and a gamma-globulin standard was used throughout this study. Bio-Gel® P-4Gel fine (Bio-Rad, wet bead size 45–90 μm, molecular weight exclusion limit of >4000) was used to separate the labeled enzyme from the free dye. The absorbance at 554 nm of the labeled enzyme solution was measured to calculate the degree of labeling (*DL*). using the following formula:

$$DL = (A_{554} \times k) / (\mu_{ext} \times C_{protein})$$

where *DL* is the moles of dye per mole of protein, A_{554} is the absorbance at 554 nm, k is a dilution factor, μ_{ext} is the molar extinction coefficient of Alexa Fluor® 546 NHS Ester at 554 nm (104,000 $cm^{-1}M^{-1}$), and $C_{protein}$ is the protein concentration (M).

4.2.3 Assessment of labeled xylanases

To compare the enzymatic activity of two xylanases, a saccharification test was investigated in the presence of cellulase mixture including Xyn III or Xyn10. The substrate, sugarcane (*Saccharum officinarum*) bagasse powder, was sieved through a 1-mm mesh and pretreated by autoclaving in 1% sodium hydroxide solution at 120 °C for 20 min. The composition was estimated as: cellulose (63 %), hemicellulose (18%), lignin (7.6%), and ash (4.0%). The bagasse (10 mg on a dry matter basis) was hydrolyzed in 0.1 M acetate buffer (pH 5.0) at 50 °C, shaking at 150 rpm. The total solution volume was 1 mL and the enzyme concentration was 3 mg/g of substrate. The enzyme composition is the same as that described later in the microscopy section. The

experiments were performed for both non-labeled and labeled xylanases. The supernatant was collected at 5, 24, 48, and 96 hours to measure D-glucose yield using a CII Test Wako kit (Wako, Osaka, Japan), and D-xylose yield using a D-xylose kit (Megazyme, Wicklow, Ireland).

4.2.4 Fluorescence microscopy of a selectively-labeled enzyme in a cellulase cocktail

Transverse sections (30-μm-thick) were cut from a stem of sugarcane harvested in Okinawa, Japan, with a microtome equipped with a freezing stage. The sections were treated in 0.5% sodium hydroxide using an oil bath at 100 °C for 1 hour. After washing thoroughly, the treated sections were used as the substrate. The enzyme mixture comprised purified components of CBH I 35 wt.%, CBH II 20 wt.%, EG I 15 wt.%, EG II 5 wt.%, EG IV 5 wt.%, BGL I 5 wt.%, BXL 5 wt.%, and Xyn III 10 wt.%. One of the enzymes was replaced with a fluorescent-labeled enzyme at a fixed ratio of 5 wt.% (total enzyme basis); for example, a system comprising labeled CBH I at 5 wt.% and non-labeled CBH I at 30 wt.%. As a comparison, Xyn III was replaced with Xyn10 to visualize the functional difference between the two xylanases.

A pretreated section was mounted on a glass slide together with a 25-μL aliquot of an enzyme mixture (~40 mg/g biomass). A cover slip was then placed on top of the specimen and sealed with nail polish to prevent water evaporating during the reaction. The preparation was performed on a thermo-stage, maintained at 50 °C, with an inverted fluorescent microscope (IX71, Olympus, Tokyo, Japan) under a constant illumination flux from a super-high pressure mercury lamp and a 4× objective lens (UPlanFLN, NA: 0.13, Olympus). Images (1600×1200 pixels, 8 bit RGB) were recorded every 5 minutes for 360 minutes in fluorescent mode with a charge-coupled device camera having an exposure time set at 500 ms (DP 73, Olympus). As the filter set, TRIRC-B (Semrock, N.Y., USA) was used comprising a bandpass excitation filter (543 nm/22 nm), a dichroic mirror (>562 nm), and a bandpass emission filter (593 nm/40 nm). No auto-fluorescence was detected in the presence of a non-fluorescent-labeled enzyme subjected to the same conditions.

4.2.5 Relationship between the number of labeled enzymes and fluorescence image intensity

Prior to image data interpretation, the relationship between the fluorescence intensity of the microscopic image and the labeled enzyme concentration was determined. A series of 2-μL enzyme-labeled solutions, at various concentrations, were placed in a circle (φ = 8 mm) surrounded by water-resistant fluororesin on a glass slide, TF0808 (MATSUNAMI, Osaka, Japan). Thereafter, a cover slip was placed on the solution and observations made by fluorescent microscopy under the same conditions as previously described. The average fluorescence intensity was calculated from five different positions using ImageJ software, and plotted against the corresponding enzyme concentration.

4.2.6 Time-lapse fluorescence profiles from two-dimensional images

A stack of fluorescent images (at 5-min intervals) were carefully aligned by the registration algorithm proposed by Thévenaz et al (1998) as a plugin for ImageJ. A 500×500 pixel region was cropped, wherein one complete vascular bundle (VB) from the inner part of the stem was recorded. After conversion to a gray-scale, and noise reduction by median filtering, the intensity profiles from each pixel in an image stack were taken as a function of time. The 250,000 time-dependent intensity profiles were then classified into eight representative profiles by the *k*-Means algorithm, and the corresponding regions associated with the eight profiles were contour-mapped into two-dimensional images. The number of clusters was chosen to be slightly larger than the number of cell-types in the region of interest: phloem, bundle sheath, metaxylem and parenchyma, which were expected to show different susceptibilities to the enzymatic attack. All calculations were performed in python 3.6 using the scikit-learn v0.19.2 (Pedregosa et al. 2011) data mining tool.

4.3 Results and discussion

4.3.1 Xylanase activity: effect of labeling

As xylanase is known to be a key enzyme for the saccharification of biomass, the investigation herein studied two endo-β-xylanases, Xyn III and Xyn10, both of which belong to the glycoside hydrolase family GH-10 in the CAZy database. Xyn III was observed by Xu et al (1998) to be a highly active xylanase enzyme, while Xyn10, developed by Kao Corporation, Tokyo, Japan (Shibata et al. 2017), exhibits an even higher activity. Xyn III has no carbohydrate-binding module (CBM) and shows a high affinity to soluble xylan (Matsuzawa et al. 2016), while Xyn10 is an endo-type xylanase with a CBM 1 that demonstrates a high affinity to the surface of crystalline cellulose (Shibata et al. 2017).

As previously reported (Shibata et al. 2017), Xyn10 demonstrated a higher activity than Xyn III against alkali-pretreated sugarcane bagasse powder (Fig. 4.1), reconfirming the excellent performance of Xyn10.

Furthermore, a remarkable finding in this study for Xyn10 is that the production of xylose precedes that of glucose, until 48 h of treatment (Fig. 1b). As part of the xylan structure is tightly bound to cellulose fibrils (Penttilä et al. 2013), effective xylanases may remove xylan from the surface of cellulose, which subsequently allows cellulose to be accessible to cellulase. Finally, the reaction progress appears to be similar for fluorescence-labeled and non-labeled enzyme systems (Fig. 4.1), indicating that the enzyme labeling does not influence on xylanase hydrolysis performance. Additionally, there was no significant influence hydrolysis performance for the other enzymes analyzed in this study (data not shown). Hence, enzyme labeling does not influence data interpretation derived from fluorescence microscopy in this study.

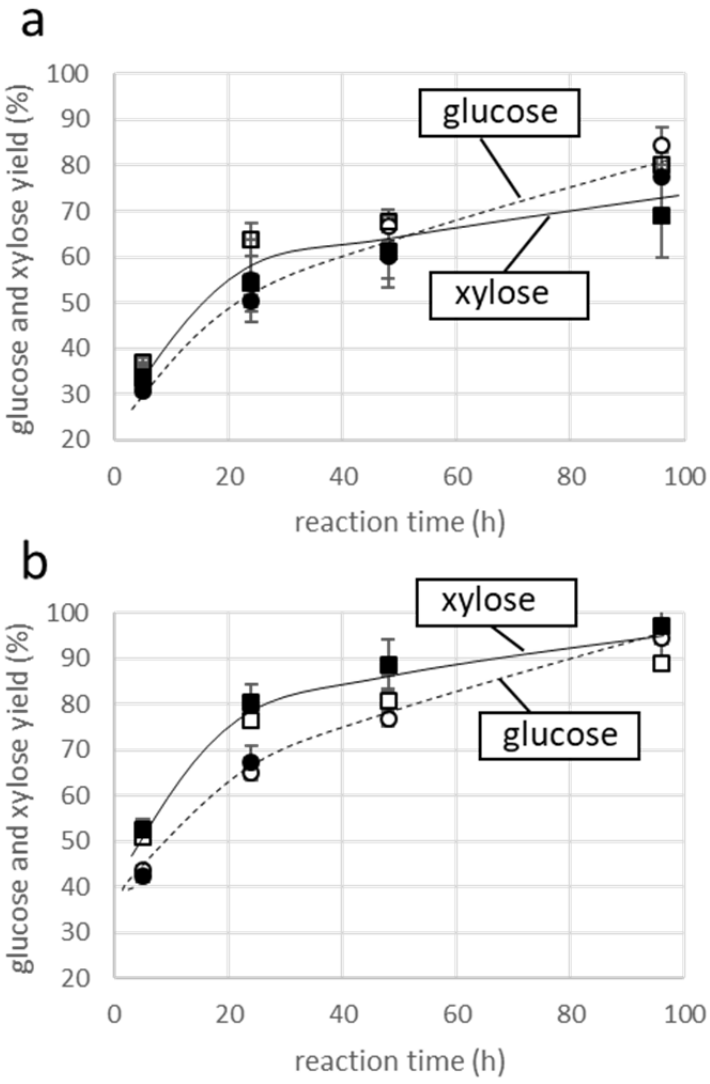

Figure 4.1 Saccharification in the presence of labeled and non-labeled enzymes. Glucose yield was calculated by measuring glucose divided by the total glucose amount expected from cellulose. Xylose yield was calculated in the same way. a) Glucose and xylose yields in the presence of labeled or non-labeled Xyn III, b) glucose and xylose yields in the presence of labeled or non-labeled Xyn10. Open circle: glucose by non-labeled xylanase, filled circle: glucose by labeled xylanase, open square: xylose by non-labeled xylanase, filled square: xylose by labeled xylanase. The error bars indicate the standard deviation of the measured values.

4.3.2 Relationship between the number of labeled enzymes and fluorescence image intensity

Fluorescence intensity of the labeled enzyme solution at various concentrations is plotted in Fig. 4.2a. Excellent linearity between the fluorescence microscopy intensities and the applied dose of individual enzymes was demonstrated. The intensity per mole of protein (the slope of each line), was calculated in Fig. 4.2a. When the slope was plotted against the degree of enzyme labeling for each enzyme (Fig. 4.2b), a linear relationship was also observed, indicating that fluorescence intensity is proportional to the number of fluorescence dye molecules regardless of the enzyme tagged. Therefore, the fluorescence intensity of each enzyme can be quantitatively compared by normalizing to *DL* of the corresponding enzyme.

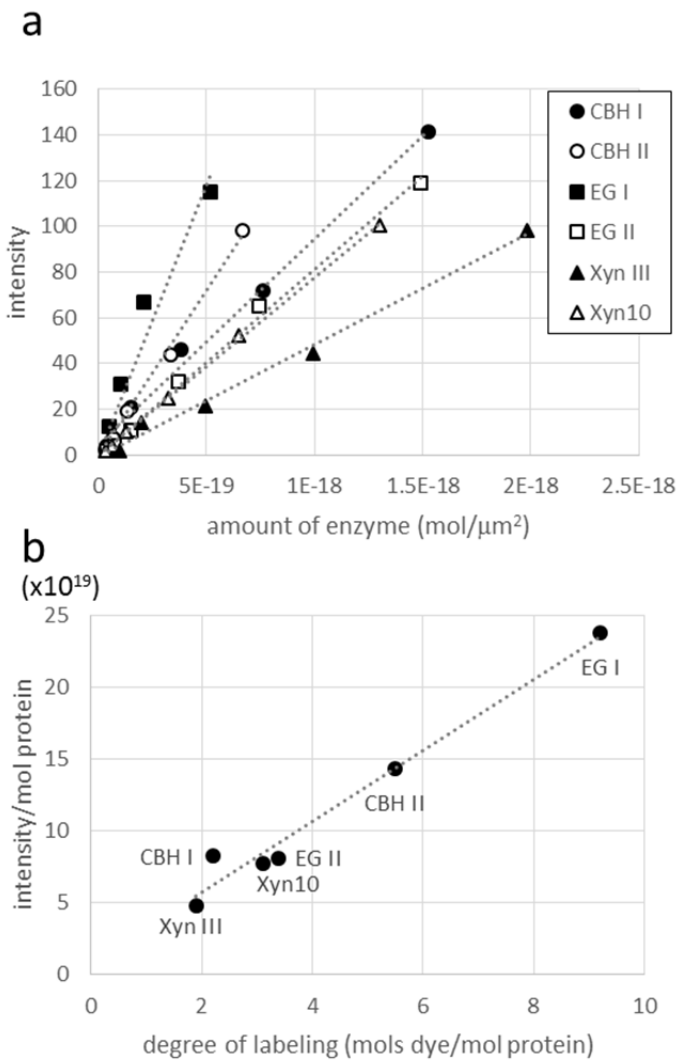

Figure 4.2 a) Relationship between image intensity and enzyme concentration. b) Relationship between intensity per mole of protein and degree of labeling.

4.3.3 Changes to morphology and enzyme adsorption during hydrolysis

The typical appearance of the VB of sugarcane during hydrolysis is presented in Fig. 4.3. The images were taken in both normal bright-field mode (Fig. 4.3a–c) and fluorescence mode (Fig. 4.3d–f). As shown in the bright field image (Fig 4.3c), the parenchyma cell wall substances distant from the VB are more susceptible to hydrolysis, and the image contrast was almost lost after 360 min of treatment. The thick-walled bundle sheath of the VB remained but became notably thinner. Initial adsorption of

CBH I occurred at the parenchyma cells distant from the VB (Fig. 4.3d) and became more concentrated toward the VB outer areas (Fig. 4.3e) after 100 min, which is composed of smaller-sized parenchyma cells and thinner-walled VB fibers. Thereafter, CBH I was observed only at highly-lignified areas such as the bundle sheath. As such, it was possible to visualize the substrate degradation pattern and the corresponding enzyme distribution.

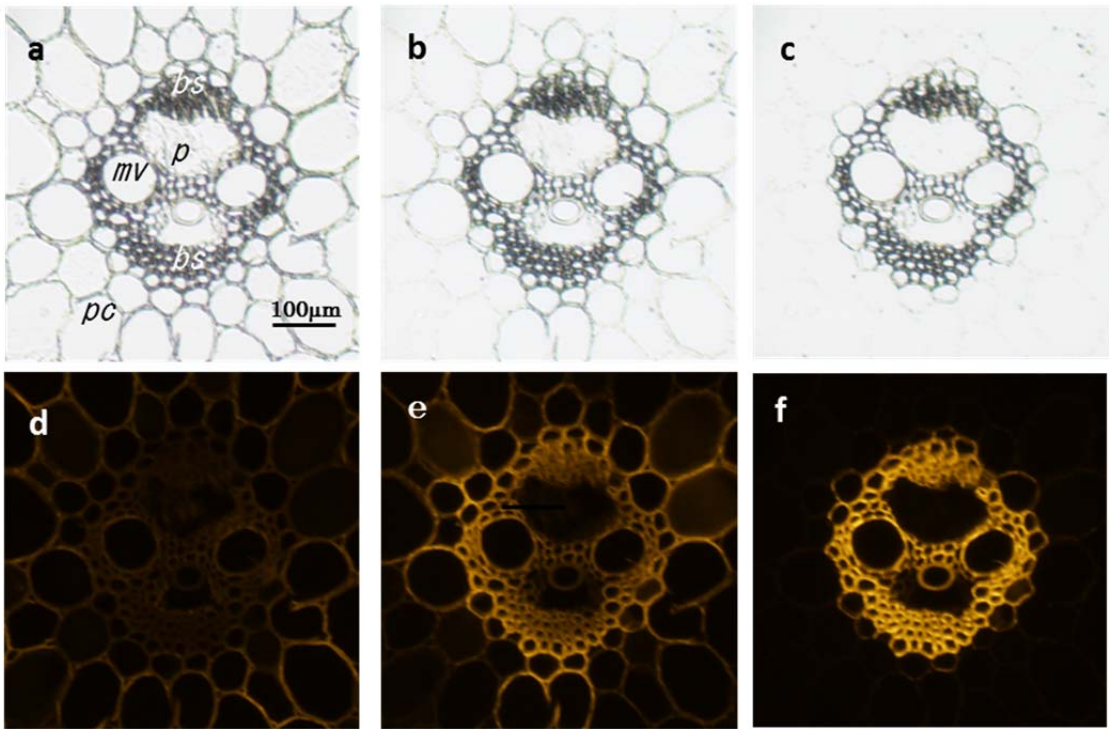

Figure 4.3 Typical microscopic images during hydrolysis in the presence of mixed enzymes containing labeled cellobiohydrolase (CBH) I. Hydrolysis time: a & d) 0 min, b) 90 min, e) 100 min, c & f): 360 min. a–c: bright field microscopy images, d–f: fluorescent microscopy images. *bs*: bundle shearth, *p*: phloem, *pc*: parenchyma, *mv*: metaxylem vessel.

4.3.4 Time-lapse analysis of individual enzymes

As a negative control, free Alexa Fluor® 546 NHS Ester were tested in the same experimental conditions. No fluorescence of dyes on sugarcane sections was

observed. A concept of the analysis is given in Fig. 4.4. A stack of images were carefully aligned, as in Fig. 4.4a. From a set of images, 250,000 intensity profiles were obtained, with some intensity profiles shown in Fig. 4.4b. Several profile patterns are clearly observed; flat profiles (background), constant increasing or decreasing profiles, profiles with maximum peak, and so on. The typical center profiles obtained by the common method of vector quantization (*k*-means clustering), are represented in Fig. 4.4c. The number of clusters was set at eight. Finally, all pixels were colored

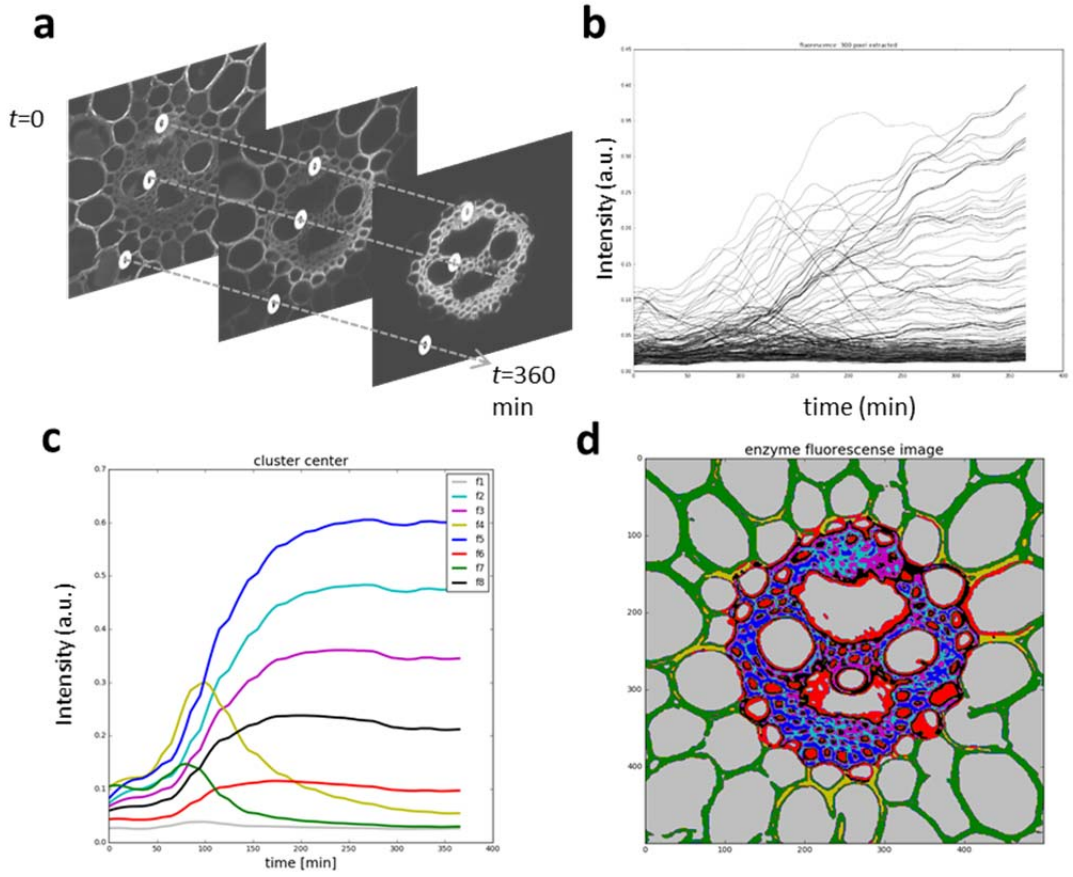

Figure 4.4 A time-lapse flow-diagram observation of enzyme localization in a sugarcane section. A stack of image slices was registered and carefully aligned (a). Intensity at each pixel point in the stack as a function of time. Up to 300 profiles randomly extracted from 250,000 profiles in total were exemplified in (b). The eight representative profiles obtained by *k*-means clustering (c) together with a typical contour map of the corresponding eight regions (d).

corresponding to the profiles (Fig. 4.4d). In this way, the adsorption/desorption behavior was analyzed in a 2D image for each labeled enzyme.

Fig. 4.5 shows the intensity profiles of each enzyme together with the 2D distribution image. To compare intensity as a function of enzyme concentration, the intensity profiles were divided by *DL*. Thereafter, the labeled enzyme was fixed at 5 wt.%, based on the total enzyme present in the system. Therefore, the intensity was converted to the actual enzyme concentration; for example, the intensity was multiplied by seven in the case of CBH I. The patterns from CBH I, CBH II, EG I, EG II, and Xyn10, were somehow similar to one another, with a pattern displaying two type of profiles having a maximum peak and simply increasing as a function of time. The profile having maximum peak derives from the area of parenchyma whose cell walls are thin and contain little lignin, or parenchyma cells of a relatively small diameter, adjacent to the VB. The simply increasing profile derives from the area of bundle sheath whose cell walls are thick and contain significant amount of lignin, and is relatively enhanced at the outer VB area. Combining the profiles and the 2D enzyme distributions, it was concluded that all enzymes, except for Xyn III, were significantly adsorbed at the parenchyma cell walls distant from the VB during the initial stage of hydrolysis. The enzymes gradually moved toward smaller parenchyma cells adjacent to the VB. Thereafter, the enzymes desorbed from the hydrolyzed parenchyma and first re-adsorbed on areas exhibiting less lignin content before finally moving to areas of the VB cell walls containing the highest degree of lignin. Conversely, the behavior of Xyn III was significantly unique. Throughout the hydrolysis, the degree of Xyn III adsorption was relatively small, especially almost zero at the parenchyma cells (Fig. 4.5e), which demonstrates a remarkably different behavior from Xyn10, which also possesses a CBM similar to the other enzymes. The different behaviors between the two xylanases tested in this study are suggested to arise from the possession of CBMs. Xyn III of *T. reesei* was reported to be initially devoid of a CBM and Xyn III, expressed with a xylan binding domain from *Streptomyces olivaceoviridis* E-86, showed higher adsorption toward insoluble xylan by a factor of two (Penttilä et al. 2013). Furthermore, when Xyn10 that initially possessed a CBM (Shibata et al. 2017) was modified to be

devoid of a CBM, Xyn10 was no longer observed to adsorb onto the substrates (data not shown). Therefore, the CBM of xylanase was found to be critical for the interaction with xylan molecules that are closely associated with cellulose molecules at the substrate surface, which may improve the total activity of the cellulase system toward biomass.

4.3.5 Time-lapse analyses of enzyme activity in specific anatomical area

Taking the maximum amount of adsorbed CBH I to be one, all the profiles in Fig. 4.5 were recalculated and the relative amounts of each enzyme in the specific anatomical area were reproduced in Fig. 4.6. The specific anatomical areas are parenchyma cells, parenchyma cells near the VB, and the outer-most cells of the VB. As shown in Fig. 4.6, the major enzyme that adsorbed on the surface of the substrate was unambiguously CBH I. Additionally, the profiles from CBH I, EG II, and Xyn10 were somehow similar in that these systems worked rapidly and moved to other regions that were more difficult to be hydrolyzed. Particularly, EG II and Xyn10 appeared to adsorb simultaneously; however, the desorption rate of Xyn10 was observed to proceed slightly quicker than EG II. Conversely, the degree of CBH II adsorption, which is known to work synergistically with CBH I (Fägerstam and Pettersson 1980; Henrissat et al. 1985), was as low as one seventh of CBH I, and furthermore, enzyme adsorption maxima occurred ~1 h later than that of CBH I. This observation may explain partly why both these CBHs are considered to be processive enzymes; however, CBH II exhibits more of a less-processive nature as postulated earlier (Boisset et al. 2000).

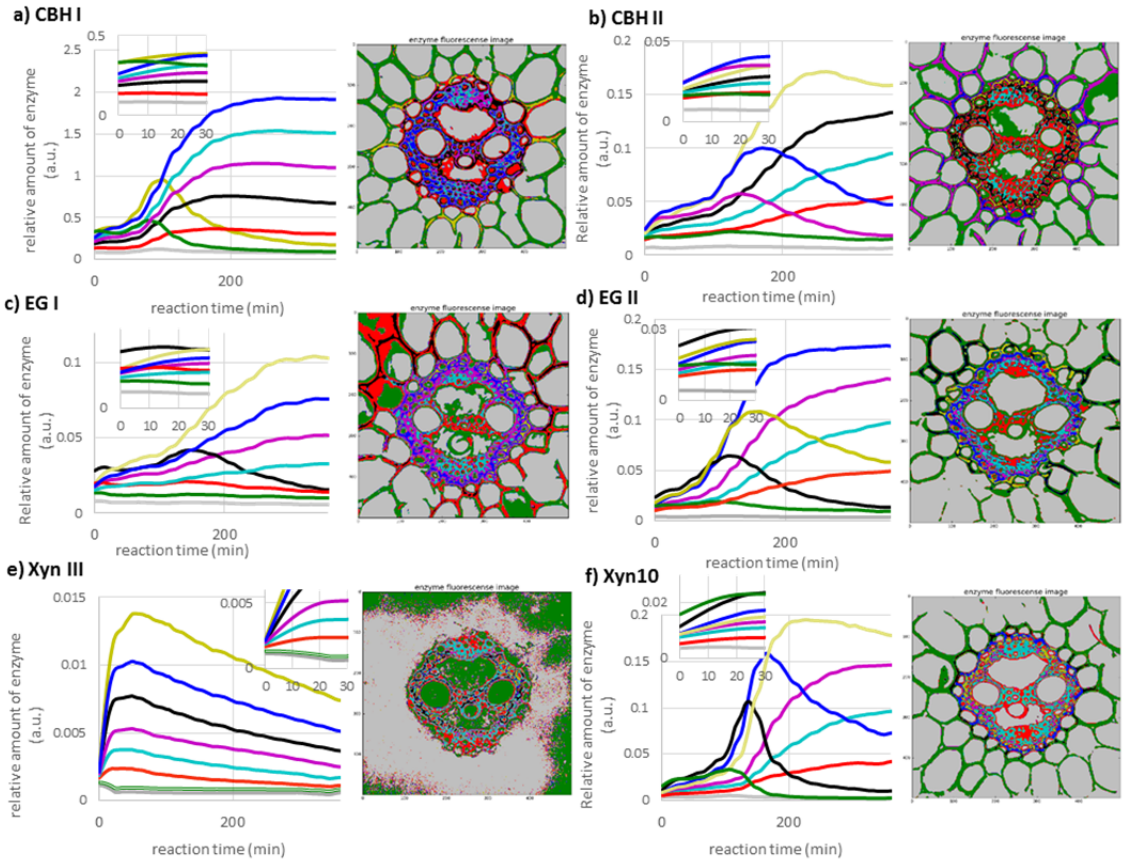

Figure 4.5 Center adsorption/desorption profiles of each enzyme, together with the corresponding contour map in the 2D image. Inserts are enlarged profiles up to 30 min.

As for EG I and EG II, significant differences in the enzyme-substrate interactions are clearly demonstrated. As EG II was adsorbed to a significantly higher degree, it is suggested that EG II functions more efficiently near the cellulosic surface, while the adsorption of EG I to parenchyma was significantly hindered (Fig. 4.6 a and b) and preferred molecules dissociated from the substrate suface. Additionally, pulp viscosity was reported to decrease to a greater extent in the presence of EG II when compared

with EG I (Rahkamo et al. 1996). Furthermore, Horikawa et al. (2016) reported that the difference in enzymatic activity between EG I and EG II toward water-soluble carboxymethyl cellulose, was not distinguishable, whereas EG II significantly decreased

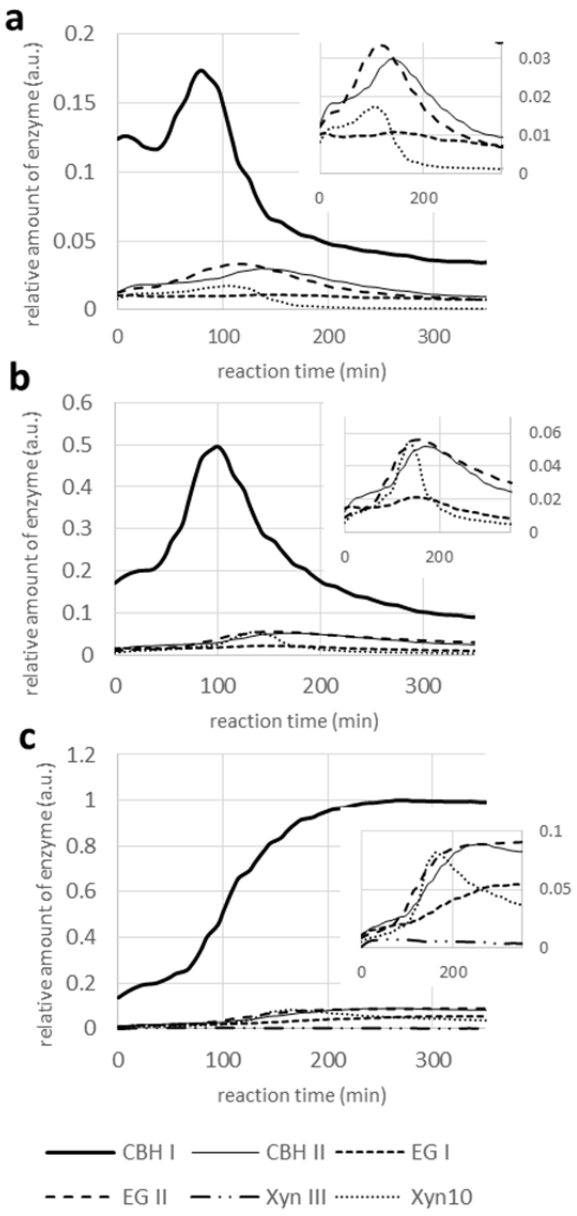

Figure 4.6 Relative enzyme adsorption/desorption profiles in each cell-type. Inserts are enlarged graphs. a) parenchyma, b) parenchyma cells near the vascular bundle, and c) the outer-most cells of the vascular bundle.

the degree of polymerization of cellulose in a microfibrillar form than EG I. These reports agree well with my binding experiment.

4.4 Conclusions

From the time-lapse analyses of the transverse sections of sugarcane stems, it is clear that CBH I is the most important and indispensable enzyme, which adsorbed onto the substrate significantly more than any other enzyme, displaying a rapid adsorption/desorption action. Conversely, even though CBH II is a processive enzyme, similar to CBH I, the observed adsorption was less than expected. EG I and EG II display different modes of action toward the microstructure of the substrate: EG II directly attacks the surface, while EG I exhibits a preference toward disentangled molecules. As for xylanases, while Xyn10, in the presence of CBM, adsorbed at the initial stage of hydrolysis and desorbed soon after, the degree of Xyn III adsorption on any tissue of sugarcane was minimal. The visualization of individual enzymes is important to elucidate the orchestrated interactions between the enzyme and the complex biomass.

4.5 List of abbreviations

CBH	cellobiohydrolase
EG	endoglucanase
BGL	β-glucosidase
Xyn	endoxylanase
BXL	β-xylosidase
DL	degree of labeling
VB	vascular bundle
CBM	carbohydrate-binding module

4.6 References

Beldman G, Voragen AG, Rombouts FM, Pilnik W (1988) Synergism in cellulose hydrolysis by endoglucanases and exoglucanases purified from *Trichoderma viride*. Biotechnol Bioeng 31:173–178. https://doi.org/10.1002/bit.260310211

Boisset C, Fraschini C, Schülein M, et al (2000) Imaging the enzymatic digestion of bacterial cellulose ribbons reveals the endo character of the cellobiohydrolase Cel6A from *Humicola insolens* and its mode of synergy with cellobiohydrolase Cel7A. Appl Environ Microbiol 66:1444–1452

Chanzy H, Henrissat B, Vuong R (1984) Colloidal gold labelling of l,4-β-D-glucan cellobiohydrolase adsorbed on cellulose substrates. FEBS Lett 172:193–197. https://doi.org/10.1016/0014-5793(84)81124-2

Fägerstam LG, Pettersson LG (1980) The 1.4-β-glucan cellobiohydrolases of *Trichoderma reesei* QM 9414: A new type of cellulolytic synergism. FEBS Lett 119:97–100. https://doi.org/10.1016/0014-5793(80)81006-4

Henrissat B, Driguez H, Viet C, Schülein M (1985) Synergism of cellulases from *Trichoderma reesei* in the degradation of cellulose. Nat Biotechnol 3:722–726. https://doi.org/10.1038/nbt0885-722

Horikawa Y, Imai T, Abe K, et al (2016) Assessment of endoglucanase activity by analyzing the degree of cellulose polymerization and high-throughput analysis by near-infrared spectroscopy. Cellulose 23:1565–1572. https://doi.org/10.1007/s10570-016-0927-9

Igarashi K, Koivula A, Wada M, et al (2009) High speed atomic force microscopy visualizes processive movement of *Trichoderma reesei* cellobiohydrolase I on crystalline cellulose. J Biol Chem 284:36186–36190. https://doi.org/10.1074/jbc.M109.034611

Igarashi K, Uchihashi T, Koivula A, et al (2011) Traffic jams reduce hydrolytic efficiency of cellulase on cellulose surface. Science 333:1279–1282. https://doi.org/10.1126/science.1208386

Jervis EJ, Haynes CA, Kilburn DG (1997) Surface diffusion of cellulases and their isolated binding domains on cellulose. J Biol Chem 272:24016–24023. https://doi.org/10.1074/jbc.272.38.24016

Kawaguchi T, Enoki T, Tsurumaki S, et al (1996) Cloning and sequencing of the cDNA encoding β-glucosidase 1 from *Aspergillus aculeatus*. Gene 173:287–288. https://doi.org/10.1016/0378-1119(96)00179-5

Kawai T, Nakazawa H, Ida N, et al (2012) Analysis of the saccharification capability of high-functional cellulase JN11 for various pretreated biomasses through a comparison with commercially available counterparts. J Ind Microbiol Biotechnol 39:1741–1749. https://doi.org/10.1007/s10295-012-1195-9

Kawamori M, Ado Y, Takasawa S (1986) Preparation and Application of *Trichoderma reesei* Mutants with Enhanced β -Glucosidase. Agric Biol Chem 50:2477–2482. https://doi.org/10.1080/00021369.1986.10867787

Liu Y-S, Luo Y, Baker JO, et al (2010) A single molecule study of cellulase hydrolysis of crystalline cellulose. In: Single Molecule Spectroscopy and Imaging III. International Society for Optics and Photonics, p 757103

Matsuzawa T, Kaneko S, Yaoi K (2016) Improvement of thermostability and activity of *Trichoderma reesei* endo-xylanase Xyn III on insoluble substrates. Appl Microbiol Biotechnol 100:8043–8051. https://doi.org/10.1007/s00253-016-7563-z

Minetoki T, Kumagai C, Gomi K, et al (1998) Improvement of promoter activity by the introduction of multiple copies of the conserved region III sequence, involved in the efficient expression of *Aspergillus oryzae* amylase-encoding genes. Appl Microbiol Biotechnol 50:459–467

Pedregosa F, Varoquaux G, Gramfort A, et al (2011) Scikit-learn: Machine Learning in Python. J Mach Learn Res 12:2825–2830

Penttilä PA, Várnai A, Pere J, et al (2013) Xylan as limiting factor in enzymatic hydrolysis of nanocellulose. Bioresour Technol 129:135–141. https://doi.org/10.1016/j.biortech.2012.11.017

Pinto R, Carvalho J, Mota M, Gama M (2006) Large-scale production of cellulose-binding domains. Adsorption studies using CBD-FITC conjugates. Cellulose 13:557–569. https://doi.org/10.1007/s10570-006-9060-5

Rahkamo L, Siika-Aho M, Vehviläinen M, et al (1996) Modification of hardwood dissolving pulp with purified *Trichoderma reesei* cellulases. Cellulose 3:153–163. https://doi.org/10.1007/BF02228798

Shibata N, Suetsugu M, Kakeshita H, et al (2017) A novel GH10 xylanase from *Penicillium* sp. accelerates saccharification of alkaline-pretreated bagasse by an enzyme from recombinant *Trichoderma reesei* expressing *Aspergillus* β-glucosidase. Biotechnol Biofuels 10:278. https://doi.org/10.1186/s13068-017-0970-2

Thevenaz P, Ruttimann UE, Unser M (1998) A pyramid approach to subpixel registration based on intensity. IEEE Trans Image Process 7:27–41. https://doi.org/10.1109/83.650848

Tsuboi H, Koda A, Toda T, et al (2005) Improvement of the *Aspergillus oryzae* enolase promoter (P-enoA) by the introduction of cis-element repeats. Biosci Biotechnol Biochem 69:206–208

Wang L, Wang Y, Ragauskas AJ (2012) Determination of cellulase colocalization on cellulose fiber with quantitative FRET measured by acceptor photobleaching and spectrally unmixing fluorescence microscopy. The Analyst 137:1319–1324. https://doi.org/10.1039/c2an15938d

White AR, Brown RM (1981) Enzymatic hydrolysis of cellulose: Visual characterization of the process. Proc Natl Acad Sci U S A 78:1047–1051

Wood TM, McCrae SI, Bhat KM (1989) The mechanism of fungal cellulase action. Synergism between enzyme components of *Penicillium pinophilum* cellulase in solubilizing hydrogen bond-ordered cellulose. Biochem J 260:37–43

Xu J, Takakuwa N, Nogawa M, et al (1998) A third xylanase from *Trichoderma reesei* PC-3-7. Appl Microbiol Biotechnol 49:718–724. https://doi.org/10.1007/s002530051237

Chapter 5 Summary

I focused on bioethanol as energy resource, visualized the interaction between biomass and enzymes, and analyzed saccharification residues, especially by fluorescence labeling.

Cellulose I is not completely saccharified to glucose at a low cellulase concentration. Thus, in this study, sugarcane cellulose saccharification residues were investigated. By analyzing the saccharification residue of sugarcane bagasse, it was found that saccharification of the cellulose surface became more difficult as the process continued. The hydrophobicity of the cellulose surface are crucial for saccharification, because the high hydrophobicity of cellulose leads to an aggregation of cellulose by hydrophobic effects, which results in a lower accessibility to cellulases.

To saccharify cellulose using enzymes, pores on the cell wall surfaces large enough for the enzymes to enter are necessary. Hornification of cellulose is a phenomenon that takes place during the drying process. Hornification involves a structural change in the cellulose that restricts the enzyme's ability to access and saccharify the cellulose. Initially, cellulases were observed on the outer surfaces and dislocations of both the ND and ODr pulp fibers. The ND and ODr fibers were then cut at dislocations into shorter fibers. It was clearly observed that, over time, cellulases penetrated the cell walls of the ND pulp fiber from the outer surface, inner surface and cracks, and remained in the cell walls. In contrast, cellulases did not penetrate the cell walls of the ODr pulp fiber and instead stayed on the cracks and ends of the shortened fibers. Water was removed by drying, and new hydrogen bonds were produced between the cellulose microfibrils. Therefore, ODr fiber does not have pores on the surfaces large enough for cellulases to enter. From the above, using biomass without drying is one of the most important steps.

Numerous cellulase cocktails (crude enzymes) have been developed to improve enzymatic activity. For this purpose, the synergy of incorporating hydrolase functionality within a cellulase cocktail is a key function. However, such synergistic action, by potentially numerous types of enzymes, on biomass tissue has not been

considered, despite the importance toward the realistic case of biomass saccharification. This study aimed to visualize the behavior of each key cellulase and hemicellulose component on biomass tissue during saccharification. Time-lapse fluorescence microscopy observations were conducted during the saccharification of a thin transverse sugarcane section to monitor enzymes that had been modified with a fluorescence dye. Statistical image analysis successfully demonstrated a unique adsorption/desorption behavior of each enzyme component. Particularly, the behavior of endoxylanase10 (Xyn10), which was recently discovered from *Penicillium* sp. as a high-performance xylanase, displayed remarkable adsorption on sugarcane tissues, which accounts for the superior activity of the cellulase mixture with Xyn10.

As above, various types of biomass from microfibrils to sugarcane tissues were investigated. The knowledges obtained in this study lead to the conclusions.

Some of causes of the low saccharification rate of cellulosic biomass:

1) The process of saccharification increases the hydrophobic planes of cellulose. High hydrophobicity causes cellulose microfibril aggregations to form and the accessibility to enzymes thus becomes low.

2) Enzymes do not enter the inside of cell walls, because the number of pores large enough decreases by drying

3) Initially, enzymes saccharify cellulose contained in such areas as parenchymas, next the enzymes move to cells containing more lignin, such as fiber cells. The enzymes remain on the cells that contain more lignin.

Acknowledgement

This thesis is a compilation of works under the supervision of Professor Junji Sugiyama at Kyoto University. I would like to express my gratitude to him for guidance and supports for a long term since I was a graduate student.

I am so grateful to Professor Keiji Takabe and Professor Takashi Watanabe, who gave me precise comments and advices.

I would like to thank Associate Professor Tomoya Imai, Assistant Professors Keiichi Baba and Suyako Tazuru in the Laboratory Biomass Morphogeneses and Information (LBMI) for their advice and encouragement.

Dr. Yoshiki Horikawa of Tokyo University of Agriculture and Technology helped me to carry out my experiments and encouraged me. I would like to thank Dr. Satoshi Kimura of the University of Tokyo for instructing fluorescence microscopy and discussions with him were very productive.

I am grateful to New Energy and Industrial Technology Development Organization (NEDO), Kao Corporation, Japan Bioindustry Association, National Institute of Advanced Industrial Science and Technology (AIST), Oji Holdings Corporation, and all members of the NEDO projects, giving me information and advice of bioethanol, enzymes, and biomass.

I would like to thank Emeritus Professor Minoru Fujita of Kyoto University for guidance at undergraduate school.

I am thankful to all members of LBMI for supporting me.

Lastly, I thank my husband, my children, my parents, and friends encouraging me.